Title
The choanoflagellate S. rosetta integrates cues from diverse bacteria to enhance multicellular development

Author
Ireland, Ella

Publication Date
2019

Peer reviewed|Thesis/dissertation

The choanoflagellate *S. rosetta* integrates cues from diverse bacteria to enhance multicellular development

By

Ella Victoria Ireland

A dissertation submitted in partial satisfaction of the
requirements for the degree of
Doctor of Philosophy
in
Molecular and Cell Biology

in the

Graduate Division

of the

University of California, Berkeley

Committee in charge:

Professor Nicole King, Chair
Professor Russell Vance
Professor Iswar Hariharan
Professor Brian Staskawicz

Fall 2019

Abstract

The choanoflagellate *S. rosetta* integrates cues from diverse bacteria to enhance multicellular development

By

Ella Victoria Ireland

Doctor of Philosophy in Molecular and Cell Biology

University of California, Berkeley

Professor Nicole King, Chair

Bacteria play critical roles in regulating animal development, homeostasis and disease. Animals are often hosts to hundreds of different species of bacteria, which produce thousands of different molecules with the potential to influence animal biology. Direct interactions between different species of bacteria, as well as the environmental context of the animal-bacteria interaction, can have a significant impact on the outcome for the animal (Chapter 1). While we are beginning to understand the role of context in bacteria-animal interactions, surprisingly little is known about how animals integrate multiple distinct bacterial inputs.

In my doctoral research I studied the choanoflagellate *Salpingoeca rosetta*, one of the closest living relatives of animals, to learn more about how eukaryotes integrate diverse bacterial cues. As with animals, bacteria regulate critical aspects of *S. rosetta* biology. The bacterium *Algoriphagus machipongonensis* produces sulfonolipid Rosette Inducing Factors (RIFs), which induce multicellular "rosette" development in *S. rosetta*. In contrast, the bacterium *Vibrio fischeri* produces a chondroitinase, EroS, which acts as an aphrodisiac and induces *S. rosetta* to undergo sexual reproduction. Thus, *S. rosetta* undergoes distinct life history transitions in response to biochemically unrelated bacterial cues. Importantly, both the choanoflagellate and its bacterial partners in these interactions can be independently cultured and manipulated in the lab. This motivated me to use *S. rosetta* as a simple model for exploring how eukaryotes are influenced by environments filled with diverse bacterial cues.

I investigated how *S. rosetta* responds to environments containing both the mating inducer EroS and the rosette-inducing RIFs (Chapter 2). I found that the initiation of mating behavior is unchanged in the presence of cues that induce rosette development. In contrast, rosette development is significantly enhanced by the presence of the mating inducer. Simultaneous exposure to RIFs and EroS elicited both larger multicellular colonies and an increase in the number of colonies. These results demonstrate that, rather than conveying conflicting sets of information, these distinct bacterial cues synergize to augment multicellular development.

Furthermore, I found that the mating cue EroS induces changes in the extracellular matrix that had previously only been observed during rosette development, suggesting one possible point of intersection for these two pathways (Appendix 1).

These findings highlight how synergistic interactions among bacterial cues can influence the biology of eukaryotes. The model eukaryote *S. rosetta* integrates cues from diverse bacteria and modulates its response accordingly. Ongoing research investigating the *S. rosetta* targets of these bacterial cues (Appendix 2) may reveal the mechanistic basis of this synergy. The experimental tractability of *S. rosetta* and its interactions with bacteria make it an exciting model system in which to investigate the question how eukaryotes sense and respond to diverse bacterial cues.

Table of Contents

List of Figures and Tables

Acknowledgements

First, I would like to thank my advisor, Nicole King. Your skill and enthusiasm for communicating your science has inspired me to give better talks, write better papers, and spread the gospel of choanos. Thank you for giving me the opportunity to explore all sides of the scientific world, through volunteering, teaching, and attending diverse conferences and courses. Finally, thank you for providing an incredibly supportive lab environment and encouraging a healthy work-life balance.

I would also like to thank my committee, Russell Vance, Iswar Hariharan and Brian Staskawicz, who provided valuable feedback and support throughout my PhD.

Thank you to the past and present members of the King lab, for making it enjoyable to come to lab every day. Thanks especially to Tera Levin, for being a fantastic rotation mentor and making me want to join the King lab, and Arielle Woznica for laying the foundation for and encouraging me to pursue this thesis project.

I was very lucky to make great friends during graduate school, and especially want to thank Kelsey Van Dalfsen and Sarah Gilbertson for encouraging me to keep going when the going got tough.

Finally, thank you to my family for supporting me throughout this very long journey. Thanks to my parents, for encouraging a love of learning from an early age and suggesting graduate school in the first place. Thank you to Tater Tot, who was there from the beginning, and Luna and Juniper, who were born during my PhD. And most importantly, thank you to Joe for having confidence in me whenever mine was waivering, and for always being there to listen to me complain about the failures and celebrate the victories.

Chapter 1

How context shapes bacteria-animal interactions

Introduction

In recent decades, research in diverse animal systems has shown that bacteria exert strong influences on animal development, from inducing larval settlement in marine invertebrates (1–4) to regulating proper development of the intestinal epithelium (5–9), immune system (10–12), and nervous system in vertebrates (13, 14). In addition to the critical roles bacteria play in animal development, bacteria also regulate animal homeostasis and disease (15). While pathogenic bacteria have been known to cause disease for well over a century (16), the roles of commensal and non-pathogenic bacteria in maintaining homeostasis have only recently been widely appreciated. Thus, many different bacteria influence animal biology in diverse ways.

The different contexts in which bacteria-animal interactions occur can determine the outcome for the animal, as both animals and their environments are complex ecosystems. Context can be viewed at multiple levels: interactions between environmental factors and bacteria, interactions among bacterial species, and integration by the animal of distinct bacterial inputs (Fig. 1.1, Table 1.1). There are many documented examples of how abiotic environmental factors, such as temperature, influence bacteria and their interactions with their eukaryotic partners (Table 1.1). Inter-bacterial interactions such as colonization resistance are also well-studied and known to influence the outcome for the animal (Table 1.1). However, little is known about how animals integrate different bacterial inputs to regulate their response. Here, we briefly review the role of environmental-bacterial and bacterial-bacterial interactions in mediating bacteria-animal interactions, then focus on what is known and yet to be learned about animal integration of bacterial cues.

Environmental factors regulating bacteria-animal interactions

Various environmental factors, including diet, the physical environment within the animal host, and the external environment, regulate the types of metabolites and molecular cues produced by bacteria. These molecules, in turn, regulate animal biology (Fig. 1.1A, Table 1.1).

Diet

The animal's diet, particularly its levels of fats and sugars, can affect which bacteria are able to colonize the gut, leading to differences in the composition of the microbial community (17–19). Once colonization is established, diet continues to influence bacteria-animal interactions, regulating bacterial metabolic pathways and gene expression. *Bacteroides thetaiotaomicron*, an intestinal commensal in mice and humans with far-reaching effects on host physiology (20), provides a good example of how diet influences the resident bacteria with outcomes for the host. Colonization of the intestine by *B. thetaiotaomicron* is inhibited by dietary fructose and glucose (21) (Table 1.1). Additionally, *B. thetaiotaomicron* expresses different capsular polysaccharides depending on which dietary carbohydrates are available (22–24). Expression of different capsular polysaccharides confers differences in fitness on

the bacterium, and different capsular polysaccharides are presented differently to T cells, suggesting that differences in dietary carbohydrates could influence how *B. thetaiotaomicron* interacts with the host immune system (10, 23, 25) (Table 1.1). Furthermore, dietary glucose regulates the expression of BT4295, a *B. thetaiotaomicron* outer membrane antigen that is recognized by CD4+ T cells. In mice fed a high glucose diet, expression of BT4295 is repressed and T cell activation is significantly reduced (26) (Table 1.1). Studies such as these have demonstrated that interactions between components of an animal's diet and its gut microbiome can have far-reaching effects on the animal host.

Internal environment

The physical environment within the animal host can also affect which bacteria are able to colonize, as well as regulate bacterial gene expression. For example, in the squid-*Vibrio* association, the bacterium *Vibrio fischeri* colonizes the light organ of the squid *Euprymna scolopes* and is hypothesized to provide its host with camouflage by bioluminescing, a processed governed by the quorum-sensing-activated *lux* operon (27, 28). The host environment selects for colonization exclusively by *V. fischeri* (29), through expression of antimicrobials and reactive oxygen and nitrogen species that eliminate other bacteria but that *V. fischeri* can downregulate, tolerate or detoxify (30–34), and sugars towards which *V. fischeri* can navigate by chemotaxis (35, 36) (Table 1.1). In addition to regulating the ability of *V. fischeri* to colonize, the environmental context of the squid light organ is critical in regulating bacterial bioluminescence. Expression of the *lux* operon is significantly reduced when *V. fischeri* is found outside of its squid host, even if the bacterium is at densities as high as those found within the light organ (37). Compared to the external environment, the environment of the light organ differs in its levels of iron, inorganic phosphate, and the redox state, all of which contribute to expression of the *lux* operon (38–40) (Table 1.1). Thus, various environmental factors within the squid mediate bacteria-host interactions, by both selecting for the bacterial partner and regulating bacterial gene expression.

External environment

The external environment also influences bacteria-animal interactions. The role of temperature is particularly well studied in insects. For example, colonization by the endosymbiotic bacterium *Wolbachia*, which affects the reproductive capabilities of its insect hosts, is inhibited at high temperatures (41) (Table 1.1). Symbiotic bacteria can also mediate positive or negative fitness effects for their insect hosts depending on the environmental temperature. In the aphid *Acyrthosiphon pisum*, infection with the symbiotic bacteria *Serratia symbiotica*, *Hamiltonella defensa* or *Regiella insecticola* has a neutral effect at 18ºC. However, after heat shock at 37.5ºC, *S. symbiotica* and *H. defensa* confer a fitness advantage, while *R. insecticola* negatively affects survival (42) (Table 1.1). Thus, external environmental factors such as temperature can have a significant impact on how bacteria influence their animal partners.

The role of inter-bacterial interactions in bacteria-animal interactions

Inter-bacterial interactions can also affect which bacteria are able to colonize animals, as well as regulate bacterial gene expression, thereby influencing the outcome for the animal host (Fig. 1.1B, Table 1.1). Much of the research in this area has focused on interactions between commensal and pathogenic bacteria. Commensal bacteria can compete with or directly inhibit the growth of pathogens, as well as regulate pathogenic gene expression, ultimately affecting the outcome of disease.

Colonization resistance

Mouse models of the intestinal microbiota have revealed a great deal about the phenomenon of colonization resistance, whereby commensal bacteria inhibit colonization by pathogens such as *Salmonella enterica* serovar Typhimurium (STm), which causes gastroenteritis. One mechanism by which the commensal microbiota lowers the ability of pathogens to infect their hosts is through production of antimicrobials called bacteriocins, which directly kill their competitors (43). For example, the Nissle 1917 strain of *Escherichia coli* (EcN), which produces a class of bacteriocins called microcins, kills STm and reduces colonization and disease burden on the host (44) (Table 1.1). Commensals also reduce STm colonization and virulence by producing short chain fatty acids (SCFAs) through carbohydrate fermentation (45). These acids contribute to colonization resistance through multiple mechanisms: the *Bacteroides*-produced SCFA propionate inhibits STm growth by disrupting intracellular pH homeostasis (46), while both propionate and butyrate downregulate expression of the *Salmonella* Pathogenicity Island 1, inhibiting invasion of host cells (47, 48) (Table 1.1). Thus, interactions between gut commensal bacteria and STm, mediated by small molecules such as bacteriocins and SCFAs, protect the host from disease.

The capacity of the intestinal microbiota to both share and compete for resources also contributes to the ability of pathogens to colonize. STm uses hydrogen (49) and sialic acid (50) released by the microbiota to fuel its growth (Table 1.1). Competition for iron is particularly important for colonization, especially under inflammatory conditions. STm uses siderophores to sequester iron, and expression of these iron-uptake scavengers is required for STm colonization and virulence (51, 52). The probiotic *E. coli* strain Nissle 1917 competes with STm using its own iron-uptake system, thereby reducing STm colonization and protecting the host from disease (53) (Table 1.1).

Bacterial gene expression

In addition to influencing which bacteria are able to colonize, inter-bacterial interactions can also regulate bacterial gene expression, with functional effects for the animal host. Cystic fibrosis (CF) is often associated with polymicrobial infections, including by *Pseudomonas aeruginosa*, *Staphylococcus aureus* and other pathogens. *P. aeruginosa* pathogenicity is influenced by co-occurring bacteria such as *Stenotrophomonas maltophilia* and *Burkholderia cenocepacia*. These opportunistic pathogens produce cis-2-unsaturated fatty acid diffusible signaling factors (DSF), which are perceived by the *P. aeruginosa* sensor kinase PA1396, leading to changes

in *P. aeruginosa* biofilm formation and antibiotic tolerance (54, 55) (Table 1.1). *P. aeruginosa* can in turn affect the pathogenicity of another co-occurring bacterium, *S. aureus*, by enhancing its susceptibility to antibiotics (56, 57) (Table 1.1). The skin and nasal commensal bacterium *Corynebacterium striatum* also regulates *S. aureus* pathogenicity through diffusible molecules. Exposure to cell-free *C. striatum* conditioned media induces a shift in *S. aureus* from a pathogen-like state to a commensal-like state through decreased expression of virulence genes, decreased hemolytic activity, and decreased fitness (58) (Table 1.1). Studies such as these demonstrate that interactions between different bacterial species can have significant effects on disease outcome in the animal host.

Integration of bacterial cues by animals

As discussed above, environmental context can affect the ways in which bacteria regulate their animal hosts, as can interactions with other bacteria. But a third, less well understood level of interaction is that of animals integrating multiple bacterial cues (Fig. 1.1C). Understanding how animals receive information from multiple bacteria encountered simultaneously is of great importance and yet remains somewhat elusive. One strong possibility is that animals integrate different cues in order to regulate their response, a phenomenon that has long been observed in the context of development. Animal development is governed by a limited number of signaling pathways, but integration of these pathways can result in diverse developmental outcomes (59, 60). This ability to synthesize information from different endogenous signals suggests that animals may also integrate bacterial cues.

Immune response

Much of the research on how animals interact with multiple species of bacteria has focused on the response of the innate immune system to commensal and pathogenic bacteria. Recent studies in mice have shown that while some commensal bacteria are required for the animal host to mount an appropriate immune response to pathogens, other commensals are not required but instead enhance the host phenotype through as-yet unknown mechanisms. For example, a defined consortium of 11 commensal species robustly induces IFNγ+ CD8 T cells to fight infection by *Listeria monocytogenes*. When the group is reduced to 4 species, IFNγ+ CD8 T cells are induced at a significantly lower level. The remaining group of 7 species does not induce at all on its own, but enhances the phenotype induced by the group of 4 (61) (Fig. 1.2A). Another class of T cells, regulatory T cells (Tregs), is robustly induced by a group of 17 Clostridia strains. Monocolonization with each of the strains induces little to no increase in Tregs, and colonization with subsets of the strains induces increases that are substantially smaller than all 17 strains together, suggesting that full Treg induction requires synergy between the 17 strains (62) (Fig. 1.2A).

The presence of multiple bacterial species can also enhance the immune response in a different animal model, *Drosophila melanogaster*. When *D. melanogaster* is co-infected with both virulent *P. aeruginosa* and other species of

bacteria that on their own are avirulent or even beneficial, there is a synergistic effect, resulting in a decrease in survival as compared to infection with *P. aeruginosa* alone. Different combinations of bacteria can have either additive, suppressive, or synergistic effects on *D. melanogaster* antimicrobial peptide expression, which contributes to the survival of the animal (63) (Fig. 1.2B).

Integration of bacterial cues also appears to regulate innate immune receptor responses. Research on conserved bacterial "microbial-associated molecular patterns" (MAMPs) has demonstrated cooperation between their target innate immune receptors in animals, such as the toll-like receptors (TLRs). Agonists for different TLRs have a synergistic effect in human and mouse dendritic cells, increasing production of the cytokines IL-12 and IL-23 and priming T helper type 1 responses (64) (Fig. 1.2C). In addition to mediating synergy between MAMPs, TLRs allow individual cells to distinguish between distinct bacterial cues. Analysis of single cells from mice has shown that upon co-stimulation with TLR2 and TLR4 agonists, individual cells displayed either a TLR2 or TLR4 profile, rather than a mixed response, which has been termed "non-integrative" processing (65) (Fig. 1.2D).

These examples demonstrate that animals can integrate and distinguish between multiple bacterial cues, which are in some cases produced by a single bacterial species (66). Animals can also integrate cues from two or more different species of bacteria. In a mouse model of nasopharyngeal colonization, *Haemophilus influenzae* and *Streptococcus pneumoniae* induce a synergistic increase proinflammatory cytokines. The mechanism of synergy is dependent on a *S. pneumoniae* pore-forming toxin and the host transcription factor NFκB, but in contrast to the studies described above, this synergy is TLR-independent (67) (Fig. 1.2E). This study shows that animals are able to integrate simultaneous cues from multiple bacteria in their environment and modify their phenotypic response accordingly.

Diverse phenotypes in marine invertebrates

Studies in marine invertebrates have also revealed the influences of multiple bacterial cues on animal biology. In the cnidarian model organism *Hydra vulgaris*, symbiotic bacteria are required for regular spontaneous body contractions, and germ-free animals have significantly reduced contraction frequency. Adding back individual bacterial species does not change contraction frequency, but groups of 5 species or conventionalization can restore it to near-normal levels. This suggests that cues from multiple bacteria are responsible for the regulation of contraction frequency, but it is unknown whether *H. vulgaris* integrates different cues from these bacteria, or whether the effect is due to interactions between the bacteria themselves (68). Interestingly, a complex microbiota is also required for fungal resistance in *H. vulgaris*, with individual species failing to confer protection, but additive and synergistic effects of co-colonization restoring resistance (69).

Another example of animals integrating cues from multiple bacteria is found in marine invertebrate larval settlement in response to biofilms. Different species of bacteria can be inductive or inhibitory to settlement, and mixed biofilms containing inductive and non-inductive bacteria reduce settlement compared to biofilms containing only inductive bacteria (70). For example, in the sea urchin *Heliocidaris*

erythrogramma, larval settlement correlates with the relative abundance of inductive and inhibitory bacteria, and larvae appear to respond to the sum of these positive and negative cues (71) (Fig. 1.3A).

Studies of the squid-*Vibrio* symbiosis have shown that in addition to inducing innate immune responses, bacterial MAMPs can synergize to regulate animal development (Fig. 1.3B). Lipopolysaccharide (LPS) from *V. fischeri* induces epithelial cell apoptosis during development of the squid light organ, but is insufficient to induce full morphogenesis (72). Another cue from *V. fischeri*, a fragment of peptidoglycan called tracheal cytotoxin (TCT), synergizes with LPS to induce normal light organ morphogenesis (73). TCT alone does not trigger apoptosis, but amplifies the low levels of apoptosis induced by LPS (73). TCT also induces epithelial regression and hemocyte infiltration, processes that are required for morphogenesis of the mature light organ (73). Studies such as these demonstrate that animals can integrate bacterial cues in order to regulate their response, and we are beginning to uncover the molecular details governing these interactions.

A simple model for studying inter-kingdom interactions

As these studies show, context plays a critical role in bacteria-animal interactions, but we still have much to learn, in particular about how animals integrate diverse bacterial cues. Mechanistic insights into these interactions have been limited by the complexity and difficulty of manipulating both the animal and the resident microbiome (74, 75), because animals are complex multicellular organisms, often hosting hundreds of different species of bacteria (76), which produce thousands of molecules that have the potential to influence the their hosts (77, 78).

Given the challenges of culturing animals and their associated microbes in isolation, complementary approaches are increasingly used to study bacteria-animal interactions. One such system is the model choanoflagellate *Salpingoeca rosetta*. Choanoflagellates are the closest living relatives of animals (79–81), and like the last common ancestor of all animals, they evolved in bacteria-rich environments (82–86). Bacteria regulate *S. rosetta* biology in myriad ways, from diet to multicellular development to mating (87, 88). Both the eukaryotic and bacterial partners in these interactions can be independently cultured and manipulated in the lab, allowing researchers to uncover the molecules and mechanisms underpinning their interactions (87, 89–91).

Thus, the study of bacteria-choanoflagellate interactions has the potential to reveal fundamental mechanisms of bacteria-animal interactions. The value of using protists as a complementary model for animal-microbe interactions has already been proven: amoebae have long been studied as a model for animal-fungal interactions, revealing fundamental mechanisms of virulence in fungal pathogens of animals (92). Importantly, bacteria that regulate *S. rosetta* biology, or their close relatives, also regulate animal biology (87, 88, 93–96). The choanoflagellate model system can therefore now be used to study how eukaryotes integrate bacterial cues, a question that remains difficult to study in animal systems.

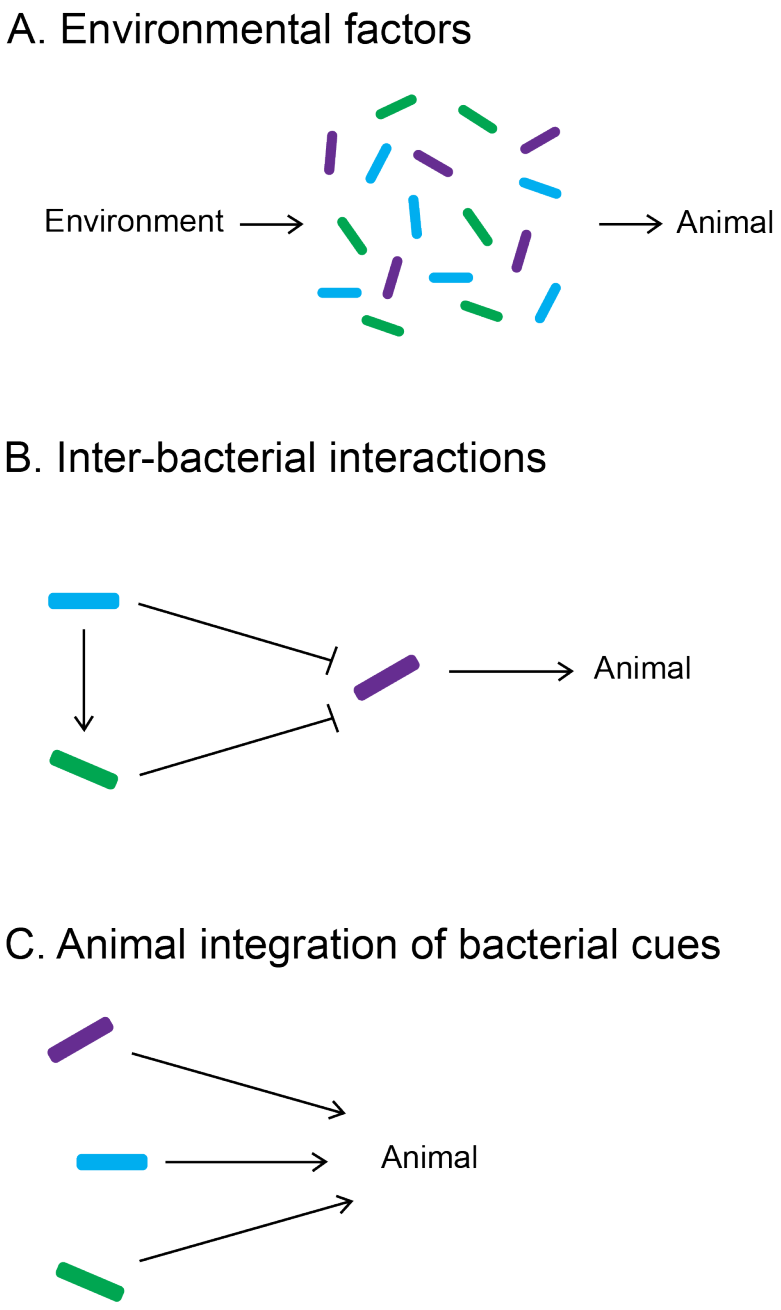

Figure 1.1: Overview of context in bacteria-animal interactions
A) Environmental factors regulate bacterial communities, which in turn regulate the biology of the animal. B) Positive and negative interactions between bacteria regulate the effect of a given bacterial species on the animal. C) Animals can also integrate distinct cues from multiple bacteria, which may be unresponsive to one another.

A

commensal bacteria	T cell response (IFNγ+ CD8 or Treg induction)
subset 1	+
subset 2	–
all species	+++

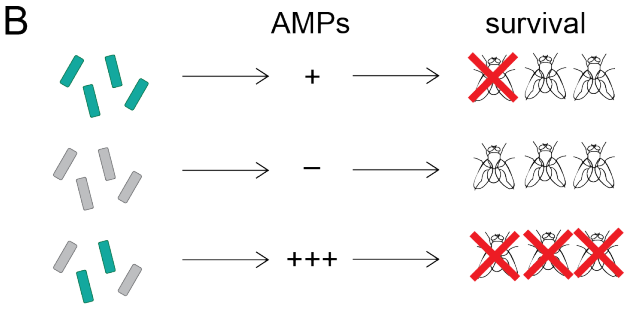

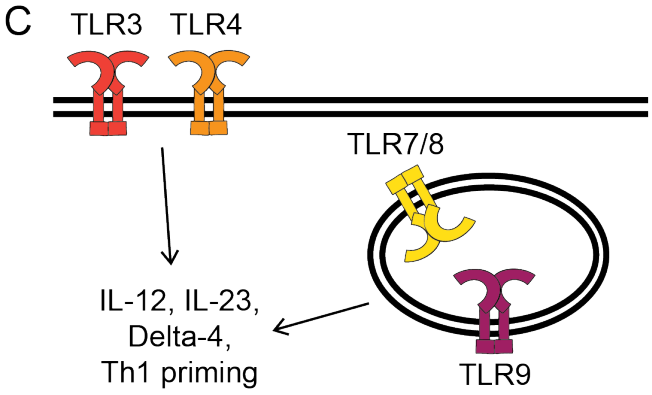

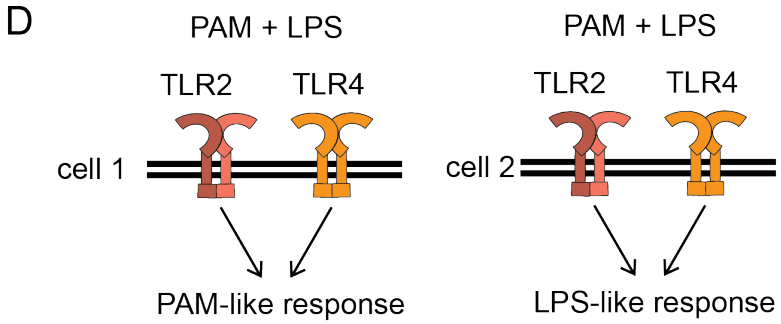

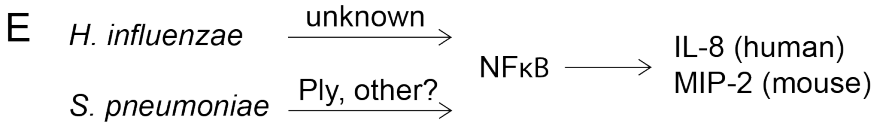

Figure 1.2: Immune responses are regulated by integration of bacterial cues
A) Synergy between commensal bacteria enhances induction of T cells. Subsets of bacteria that do not induce IFNγ+ CD8 T cells or regulatory T cells (Tregs) on their own synergize with subsets of bacteria that induce T cell responses at much lower levels. B) Polymicrobial infections induce additive, suppressive or synergistic immune responses in Drosophila. Species of bacteria that on their own do not affect antimicrobial peptide production (AMPs) or fly survival synergize with species that do. C) In dendritic cells, TLR3 and TLR4 synergize with TLR7/8 and TLR9 to enhance T helper 1 cell priming, by increasing production of cytokines IL-12 and IL-

23 and the Notch ligand Delta-4. D) Individual cells discriminate between the TLR-2 stimulus Pam3CSK4 (PAM) and the TLR-4 stimulus lipopolysaccharide (LPS), initiating a response that is either PAM-like or LPS-like, rather than a mixed response. E) *Haemophilus influenzae* and *Streptococcus pneumoniae* synergize through NFκB to increase expression of pro-inflammatory cytokines (IL-8 in humans and MIP-2 in mice) during nasopharyngeal co-colonization.

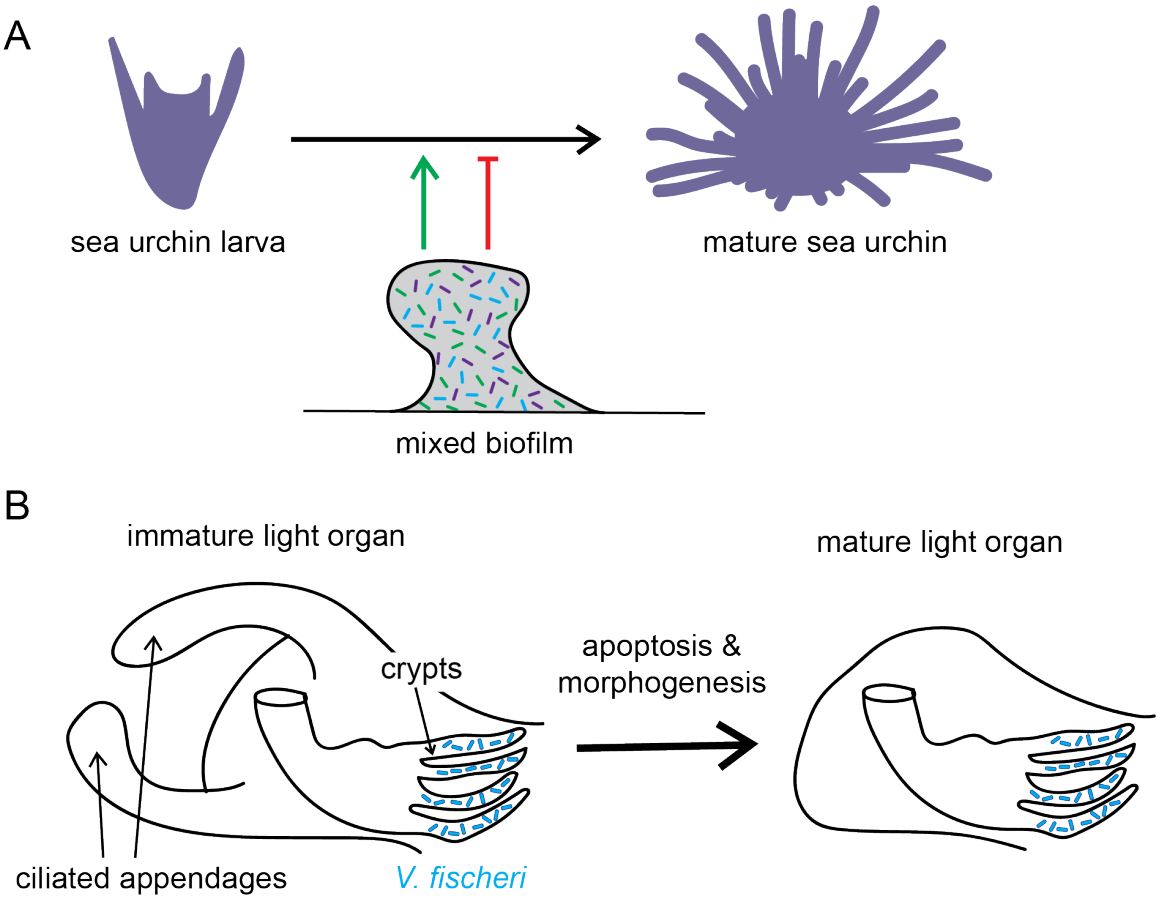

Figure 1.3: Integration of bacterial cues regulates diverse phenotypes in marine invertebrates
A) Marine invertebrate larvae respond to positive and negative cues from mixed biofilms to determine whether to undergo settlement and metamorphosis. B) *Vibrio fischeri* colonizes the crypts of the bobtail squid light organ (left), where it releases lipopolysaccharide (LPS) and tracheal cytotoxin (TCT). LPS and TCT synergize to induce apoptosis and morphogenesis of the mature light organ (right).

Table 1.1: Environmental and inter-bacterial context regulates host-microbe interactions

	Contextual cue	Bacteria	Bacterial phenotype	Host	Host phenotype	Reference
Diet	Increase in fructose + glucose	*Bacteroides thetaiotaomicron*	Decrease in colonization	Mouse	Many (e.g. nutrient absorption, obesity, immune response, development)	(20, 21)
	Carbohydrates	*Bacteroides thetaiotaomicron*	Capsular polysaccharide expression, fitness	Mouse	Immune response (potential)	(22–24)
	Increase in glucose	*Bacteroides thetaiotaomicron*	Decrease in outer membrane antigen expression	Mouse	Reduced T cell activation	(26)
Internal (host) environment	Antimicrobials (incl. ROS/NO)	*Vibrio fischeri*	Colonization	Squid	Bioluminescent camouflage	(28–33)
	Sugars	*Vibrio fischeri*	Colonization	Squid	Bioluminescent camouflage	(34, 35)
	Low iron	*Vibrio fischeri*	Increased *lux* operon expression	Squid	Bioluminescent camouflage	(38)
	Low inorganic phosphate	*Vibrio fischeri*	Increased *lux* operon expression	Squid	Bioluminescent camouflage	(37)
	Redox state	*Vibrio fischeri*	*lux* operon expression	Squid	Bioluminescent camouflage	(37, 39)
External environment	Increased temperature	*Wolbachia*	Decreased colonization	Spider mite	Reproductive capability	(40)
	Increased temperature	*Serratia symbiotica*, *Hamiltonella defensa*	Unknown	Aphid	Increase in fitness	(41)
	Increased temperature	*Regiella insecticola*	Unknown	Aphid	Decrease in fitness	(41)
Other bacteria	*Escherichia coli* Nissle 1917 bacteriocin	*Salmonella enterica* serovar Typhimurium	Decreased colonization	Mouse	Gastroenteritis	(43)
	Short chain fatty acids produced by commensal bacteria	*Salmonella enterica* serovar Typhimurium	Decreased colonization, *Salmonella* Pathogenicity Island 1 expression	Mouse	Gastroenteritis	(45–47)
	Competition with commensal bacteria for hydrogen	*Salmonella enterica* serovar Typhimurium	Decreased colonization	Mouse	Gastroenteritis	(48)

	Contextual cue	Bacteria	Bacterial phenotype	Host	Host phenotype	Reference
Other bacteria	Competition for sialic acid	*Salmonella enterica* serovar Typhimurium	Decreased colonization	Mouse	Gastroenteritis	(49)
	Competition for iron	*Salmonella enterica* serovar Typhimurium	Decreased colonization	Mouse	Gastroenteritis	(50–52)
	Stenotrophomonas maltophilia + *Burkholderia cenocepacia* diffusible signaling factors	*Pseudomonas aeruginosa*	Increased antibiotic resistance	Human/ mouse	Cystic fibrosis	(53, 54)
	Pseudomonas aeruginosa	*Staphylococcus aureus*	Decreased antibiotic resistance	Human/ mouse	Cystic fibrosis	(55, 56)
	Corynebacterium striatum diffusible molecules	*Staphylococcus aureus*	Decreased pathogenicity	Human/ mouse	Cystic fibrosis	(57)

Chapter 2

Synergistic cues from diverse bacteria enhance multicellular development in a choanoflagellate

The results presented here were published as part of the following paper:
Ireland EV, Woznica A, King N. 2019. Synergistic cues from diverse bacteria enhance multicellular development in a choanoflagellate. bioRxiv https://doi.org/10.1101/851824.

Abstract

Bacteria regulate the life histories of diverse eukaryotes, but relatively little is known about how eukaryotes interpret and respond to multiple bacterial cues encountered simultaneously. To explore how a eukaryote might respond to a combination of bioactive molecules from multiple bacteria, we treated the choanoflagellate *Salpingoeca rosetta* with two sets of bacterial cues, one that induces mating and the other that induces multicellular development. We found that simultaneous exposure to both sets of cues enhanced multicellular development in *S. rosetta*, eliciting both larger multicellular colonies and an increase in the number of colonies. Thus, rather than conveying conflicting sets of information, these distinct bacterial cues synergize to augment multicellular development. This study demonstrates how a eukaryote can integrate and modulate its response to cues from diverse bacteria, underscoring the potential impact of complex microbial communities on eukaryotic life histories.

Importance

Eukaryotic biology is profoundly influenced by interactions with diverse environmental and host-associated bacteria. However, it is not well understood how eukaryotes interpret multiple bacterial cues encountered simultaneously. This question has been challenging to address because of the complexity of many eukaryotic model systems and their associated bacterial communities. Here, we studied a close relative of animals, the choanoflagellate *Salpingoeca rosetta*, to explore how eukaryotes respond to diverse bacterial cues. We found that a bacterial chondroitinase that induces mating on its own can also synergize with bacterial lipids that induce multicellular "rosette" development. When encountered together, these cues enhance rosette development, resulting in the formation of more rosettes, each containing more cells than rosettes that form in the absence of the chondroitinase. These findings highlight how synergistic interactions among bacterial cues can influence the biology of eukaryotes.

Introduction

Eukaryotes, including animals and their closest living relatives, choanoflagellates, encounter abundant and diverse bacteria in the environment (4, 82, 97). However, interactions among eukaryotes and bacteria can be challenging to study in animal models due to the complex physiology of the hosts and the large number of oftentimes unculturable bacteria present, each of which releases diverse molecules (74, 76, 77). Multiple types of intestinal bacteria are required to induce full immune maturation in mice and humans, but it remains unclear whether this is due to interactions among the bacteria, or the integration by the host of multiple independent bacterial cues (9, 11, 61, 62, 98). The interaction of a eukaryote with multiple partners can change the magnitude or directionality of each pair-wise interaction (99), and it can be challenging to measure the functional and fitness effects of such complex networks (100). Therefore, simpler model systems may be necessary to investigate how animals and other eukaryotes integrate information from multiple bacterial cues encountered at the same time.

The choanoflagellate *Salpingoeca rosetta* can serve as a simple model for studying interactions between bacteria and eukaryotes. Like all choanoflagellates, *S. rosetta* captures bacterial prey from the water column using an apical "collar complex" composed of a microvillar collar surrounding a single flagellum (Fig. 2.1A; (101, 102)). In addition, like many animals (3, 4, 103), *S. rosetta* undergoes important life history transitions in response to distinct bacterial cues. For example, a secreted bacterial chondroitinase called EroS (for Extracellular Regulator of Sex) produced by *Vibrio fischeri*, *Proteus vulgaris,* and select other Gammaproteobacteria induces solitary *S. rosetta* cells to gather into mating swarms (Fig. 2.1B; (87)). The cells in mating swarms are not stably adherent and eventually resolve into pairs of cells that mate by undergoing cell and nuclear fusion, followed by meiotic recombination. When exposed to a different type of bacterial cue, specific sulfonolipids called RIFs (for Rosette Inducing Factors) from the Bacteroidetes bacterium *Algoriphagus machipongonensis,* solitary cells of *S. rosetta* undergo serial rounds of cell division without separation, thereby resulting in the development of multicellular rosettes of cells (Fig. 2.1C) that are physically linked by cytoplasmic bridges and a shared extracellular matrix (88, 89, 104, 105).

Mating and rosette development in *S. rosetta* differ in many respects, including the chemical nature of the bacterial cues (a protein versus lipids) and the underlying cell biology (cell aggregation versus incomplete cytokinesis). Moreover, the time scales of these processes differ, with mating swarms forming within 0.5 hours of EroS treatment (87), while definitive rosettes require multiple rounds of cell division and are not observed until 11 - 24 hours after exposure to RIFs (88, 89, 104, 105).

Motivated by the existence of distinct *S. rosetta* life history transitions that can be regulated by biochemically unrelated bacterial cues, we used *S. rosetta* as a simple model for exploring how eukaryotes are influenced by environments filled with diverse bacterial cues. We investigated how *S. rosetta* responds to environments containing both the mating inducer EroS and the rosette-inducing RIFs. We found that the initiation of mating behavior is unchanged in the presence

of cues that induce rosette development. In contrast, rosette development is significantly enhanced by the presence of the mating inducer, revealing that *S. rosetta* integrates information from seemingly unrelated bacterial cues during rosette development.

Results

Rosettes swarm in response to the EroS$_{Pv}$ mating factor

In a culture containing *S. rosetta* and the prey bacterium *Echinicola pacifica* (together comprising a culture called SrEpac; (106, 107)), solitary cells proliferated rapidly, but underwent no other observable cell state transitions (Fig. 2.1A). When the SrEpac culture was treated with the secreted bacterial chondroitinase EroS from *P. vulgaris* (EroS$_{Pv}$), *S. rosetta* cells formed mating swarms of 2-50 cells within 0.5 hours (Fig. 2.1B, Table 2.1), as previously reported (87). In contrast, treatment of SrEpac with *A. machipongonensis* RIFs contained in outer membrane vesicles (RIF-OMVs) induced development of multicellular rosettes within 24 hours (Fig. 2.1C, D, Table 2.1; (88, 89)).

We then tested how mature rosettes (formed in response to pre-treatment with RIF-OMVs for 24 hours) would respond to the mating inducer EroS. After treatment with EroS$_{Pv}$ for 0.5 hours, the pre-formed rosettes gathered into swarms that were quantifiable by their increase in area (median = 58.7 μm^2, interquartile range = 21.6-98.0 μm^2) as compared to untreated rosettes (median = 35.5 μm^2, interquartile range = 17.8-65.9 μm^2) (Fig. 2.1D-F, Table 2.1). Therefore, rather than being mutually exclusive, the rosette morphology induced by RIF-OMVs and the swarming behavior induced by EroS$_{Pv}$ are compatible. This indicates that cells in a life history stage induced by one bacterial cue (in this case RIF-OMVs) can respond to a second bacterial cue (EroS$_{Pv}$). Swarms of choanoflagellate rosettes have not previously been reported, to our knowledge, and their ecological relevance is unknown.

The mating inducer EroS$_{Pv}$ enhances rosette development

We next investigated how single-celled *S. rosetta* in an SrEpac culture would respond to simultaneous exposure to EroS$_{Pv}$ and RIF-OMVs. SrEpac cultures treated solely with RIF-OMVs for 0.5 hours, considerably less time than that required for rosette development, did not produce swarms and were indistinguishable from untreated SrEpac cultures (Fig. 2S1A-C', Table 2.1; (87, 88)). Moreover, when SrEpac cultures were treated simultaneously with EroS$_{Pv}$ and RIF-OMVs for 0.5 hours, the cells swarmed and the culture was indistinguishable from one treated with EroS$_{Pv}$ alone (Fig. 2S1A, D-E', Table 2.1). Therefore, RIF-OMVs do not appear to influence the swarm-inducing activity of EroS$_{Pv}$ over time scales of 0.5 hours or less.

In contrast, when SrEpac cultures were co-treated with RIF-OMVs and EroS$_{Pv}$ for 24 hours (long enough for rosettes to develop), the percentage of cells in rosettes increased markedly compared to cultures treated with RIF-OMVs alone (Fig. 2.2A, Table 2.1). Thus, EroS$_{Pv}$ enhances the rosette-inducing activity of RIF-OMVs. The enhancing activity of EroS$_{Pv}$ derived, in part, from the increased sensitivity of the culture to RIF-OMVs, allowing for rosette development at RIF-OMV concentrations that would otherwise fail to elicit rosette development. For example, at a nearly 10^{-6}

dilution of RIF-OMVs, no rosettes were detected in the RIF-OMV alone condition, while 4.5±0.8% (mean ± S.D.) of the cells in cultures co-treated with EroS$_{Pv}$ and RIF-OMVs were found in rosettes (see circle #1, Fig. 2.2A). In addition, when cells were exposed to saturating concentrations of RIF-OMVs (dilutions ≥3.7×10^{-4}), co-treatment with EroS$_{Pv}$ increased the percentage of cells in rosettes from a maximum of 83.6±6.8% (mean ± S.D.) in cultures that were treated with RIF-OMVs alone to 92.6±0.3% (mean ± S.D.) in cultures co-treated with RIF-OMVs and EroS$_{Pv}$ (see circle #2, Fig. 2.2A).

Enhancement of rosette development by the mating factor EroS was unexpected, and we next sought to understand the phenomenon in greater detail. To that end, we optimized a method for reproducibly inducing rosette development at low levels. Treating SrEpac with a 1:20,000 dilution of RIF-OMVs drove only a small percentage of cells (1-20%) into rosettes (Fig. 2.2A, Fig. 2S2A) and thereafter formed the basis of a "sensitized rosette induction assay" in which we could quantify the influence of EroS$_{Pv}$. Under the conditions of the sensitized rosette induction assay, we found that EroS$_{Pv}$ enhanced rosette development in a concentration-dependent manner that saturated at 0.05 U/mL (Fig. 2S2B). Using this sensitized rosette induction assay across a time series, the rosette enhancing activity of EroS$_{Pv}$ at the population level became more evident (Fig. 2S2C). For example, while treatment of SrEpac with 1:20,000 RIF-OMVs yielded only 23.4±4.9% (mean ± S.D.) of cells in rosettes at 39-hours post-treatment, co-treatment with 1:20,000 RIF-OMVs and 0.05 U/mL EroS$_{Pv}$ yielded 88.2±2.7% (mean ± S.D.) of cells in rosettes (Fig. 2.2B).

These data demonstrated that co-treatment with EroS$_{Pv}$ increases the percentage of cells in rosettes at a population level but did not reveal whether EroS$_{Pv}$-mediated enhancement works by (1) increasing the overall number of rosettes, (2) increasing the average number of cells per rosette, or (3) both. To test whether co-treatment with EroS$_{Pv}$ increased the number of rosettes formed, we induced SrEpac with either RIF-OMVs alone or RIF-OMVs + EroS$_{Pv}$ and measured the ratio of rosette colonies to solitary cells. Co-treatment with RIF-OMVs and EroS$_{Pv}$ in the sensitized rosette induction assay consistently increased the ratio of rosette colonies to solitary cells throughout the time series. For example, at 39 hours post-treatment, the ratio of rosettes to solitary cells after co-treatment with RIF-OMVs and EroS$_{Pv}$ was 0.96±0.31 (mean ± S.D.), compared to 0.06±0.02 (mean ± S.D.) after treatment with RIF-OMVs alone (Fig. 2.2C). The ratio of rosettes to solitary cells eventually plateaued, likely due to both solitary cells and rosettes (which can divide by fission (104)) dividing at the same rate. To test whether rosette size is influenced by co-treatment with EroS$_{Pv}$, we used the sensitized rosette induction assay to compare the number of cells per rosette in cultures treated with RIF-OMVs alone to those treated with RIF-OMVs and EroS$_{Pv}$. Cultures co-treated with EroS$_{Pv}$ formed larger rosettes (with 8.9±2.7 (mean ± S.D.) cells per rosette colony at 39-hours post-treatment) compared with those treated with RIF-OMVs alone (5.3±1.7 (mean ± S.D.) cells per rosette colony at the same time point) (Fig. 2.2D). Importantly, co-treatment with EroS did not affect the growth rate or cell density of cultures (Fig. 2S2D), indicating that the increase in cell number per rosette was not due to a difference in cell division rates. Therefore, at limiting concentrations of RIF-OMVs, EroS$_{Pv}$ enhances the rosette-inducing activity of RIF-OMVs in at least two ways: at

the population level, by increasing sensitivity to RIFs and the number of cells that initiate rosette development, and at the level of development, by increasing the maximal size of rosettes.

Purified RIFs and EroS are sufficient for enhancement of rosette induction

Because *A. machipongonensis* OMVs contain a suite of proteins, sugars, the sulfonolipid RIFs, and diverse other lipids, we next explored whether RIFs are sufficient for $EroS_{Pv}$-mediated enhancement of rosette development or whether the phenomenon requires a non-RIF. For example, certain lysophosphatidylethanolamines (LPEs), lipids found alongside RIFs in *A. machipongonensis* OMVs, synergize with RIFs and enhance rosette induction, in part by increasing the resistance of larger rosettes to shear forces (89).

To test whether $EroS_{Pv}$ acts synergistically with RIFs or requires other components of RIF-OMVs, we compared rosette development in SrEpac cultures treated with high-performance liquid chromatography (HPLC)-purified RIFs (88, 89) with that in cultures co-treated with HPLC-purified RIFs and $EroS_{Pv}$. Co-treatment with $EroS_{Pv}$ and purified RIFs caused a significant increase in the percentage of cells in rosettes compared to purified RIFs alone, indicating that the enhancement does not require other components of *A. machipongonensis* OMVs (Fig. 2.3A). Moreover, enhancement of rosette development was not restricted to *P. vulgaris* EroS. Co-treatment with purified *V. fischeri* EroS ($EroS_{Vf}$) also significantly enhanced RIF-OMV-induced rosette development (Fig. 2.3B), revealing that the enhancing activity likely stems from the chondroitinase activity conserved between $EroS_{Vf}$ and $EroS_{Pv}$ rather than from a lineage-specific feature found only in $EroS_{Pv}$. These findings show that simultaneous exposure to just two bacterial cues, RIFs and EroS, is sufficient to induce enhanced development of rosettes in *S. rosetta.*

Discussion

We have shown here that the choanoflagellate *S. rosetta* can sense and respond to a mix of bacterial cues, each of which in isolation induces a seemingly disparate life history transition – mating or multicellularity. Together, these cues enhance multicellular development, increasing the number of cells in rosettes at a population level by increasing the proportion of rosettes to single cells and by increasing the number of cells per rosette (Fig. 2.2 and 2.4).

The *S. rosetta* targets for EroS and the sulfonolipid RIFs are as-yet unknown (87, 88), making it challenging to infer the specific mechanisms by which EroS might enhance rosette development. One possibility is that EroS may modify chondroitin sulfate proteoglycans through its chondroitinase activity, thereby improving access of RIF receptors to RIFs, potentially explaining the increased sensitivity of EroS-treated *S. rosetta* to RIF-OMVs (Fig. 2.2A). This type of mechanism would resemble the regulation of vascular endothelial growth factor receptor 2 (VEGFR2), whose activity is inhibited by *N*-glycosylation; enzymatic digestion of glycans on VEGFR2 enhances its response to the VEGF ligand (108).

In addition to increasing the sensitivity of *S. rosetta* to RIF-OMVs, EroS treatment also resulted in rosettes that contained more cells (Fig. 2.2D). A link between rosette

size and extracellular matrix (ECM) modification was previously reported for another colony-forming choanoflagellate, *Salpingoeca helianthica*, in which treatment with a bovine chondroitinase resulted in a significantly increased number of cells per rosette (109). Furthermore, chemical perturbations of the *S. rosetta* ECM and computational modeling have shown that the material properties of the ECM, such as stiffness and volume, exert a physical constraint on rosette volume and morphology (110). Thus, EroS digestion of chondroitin sulfate in the *S. rosetta* ECM may relax these constraints and allow for increased proliferation of cells within rosettes.

Might *S. rosetta* in nature actually encounter the disparate types of bacteria that induce multicellularity and mating? Rosette development can be induced by diverse genera of marine bacteria, ranging from *A. machipongonensis*, which was co-isolated with *S. rosetta,* to *Zobellia uliginosa*, a macroalgal commensal (88, 111, 112). Likewise, mating can be induced by diverse *Vibrio* species (87), which are widespread in marine environments (113, 114). Moreover, the bioactive molecules produced by *A. machipongonensis* and *V. fischeri* (sulfonolipid RIFs and EroS) are secreted and are potent at ecologically relevant concentrations (femtomolar to nanomolar) that are comparable to those of other soluble marine signaling molecules (4, 87–89). Taken together, the diversity and abundance of rosette-inducing and mating-inducing bacteria, and the potency of the molecules they produce, argue that RIFs and EroS could be simultaneously encountered by *S. rosetta* in nature. The synergy between these cues allows *S. rosetta* to sense and respond to significantly lower concentrations of rosette-inducing factors than it could otherwise (Fig. 2.2A), contributing to the plausibility that the enhanced rosette induction they elicit could be ecologically relevant.

Simple host-microbe interactions, in which a single bacterium elicits a clear phenotype from a eukaryotic host, have begun to reveal the molecular mechanisms by which bacteria influence the biology of eukaryotes. For example, *V. fischeri* colonizes and is sufficient to induce the development of the light organ in the bobtail squid, but this process only happens through the integration of multiple cues produced by *V. fischeri* – peptidoglycan and lipopolysaccharide (73). Likewise, we have previously shown that two types of molecules – sulfonolipid RIFs and specific LPEs – are necessary to recapitulate the rosette-inducing activity of live *A. machipongonensis* (89). Thus, interactions that are seemingly simple at the organismal level – one bacterium and one eukaryote – can require complex interactions at the molecular level.

Given the underlying molecular complexity of interactions involving only one bacterium and one eukaryote, interactions among larger numbers of species are, perhaps unsurprisingly, complex and can yield a variety of outcomes, including synergistic effects (99). For example, arbuscular mycorrhizal fungi and rhizobia bacteria individually confer beneficial effects on plants, and the simultaneous presence of both groups in a tripartite association enhances these effects, increasing plant biomass to a greater extent than each partner could alone (115). Synergistic effects have also been demonstrated in interactions among eukaryotes and multiple bacterial species, such as in polymicrobial infections. Direct interactions among pathogens in polymicrobial infections (through metabolite exchange, signaling

molecules, or direct contact) can synergistically increase the disease burden for the host (such as by increasing antibiotic resistance or virulence factor expression) (116). Eukaryotic integration of bacterial cues has also been observed in the mammalian immune system, in which immune receptors such as Toll-like receptors, T cell receptors and co-receptors, each of which recognizes different bacterial ligands, synergize to enhance the response to multiple bacterial cues (66, 117).

Our finding that isolated cues from diverse environmental bacteria can synergize to enhance rosette development in *S. rosetta* (Fig. 2.3) demonstrates that this type of integration can occur at the level of the eukaryote, without requiring direct interactions among environmental bacteria. In the future, identifying the *S. rosetta* target(s) of RIF and EroS activity will likely provide detailed insights into the molecular mechanisms underlying EroS-mediated enhancement of rosette development. The experimental tractability of *S. rosetta* and its susceptibility to the influences of environmental bacteria render it an exciting system in which to investigate the mechanisms by which eukaryotes grapple with a noisy and information-rich bacterial world.

Materials and Methods

Choanoflagellate culturing conditions

Artificial seawater (ASW) was prepared by diluting 32.9 g Tropic Marin sea salts in 1L water for a salinity of 32-37 parts per thousand (107). Sea Water Complete media (SWC) was prepared by diluting 5 g/L peptone, 3 g/L yeast extract, and 3 mL/L glycerol in ASW (107). SrEpac (*Salpingoeca rosetta* co-cultured with the prey bacterium *Echinicola pacifica*, ATCC PRA-390; (107)) was cultured in 5% Sea Water Complete media (5% SWC vol/vol in ASW) at 22ºC. Cultures were passaged daily, 1 mL into 9 mL fresh media in 25cm^2 cell culture flasks (Corning). Prior to rosette or swarm induction, cultures were diluted to 1×10^5 choanoflagellate cells/mL in 5% SWC and 100 µL volumes were aliquoted into a 96-well plate (Corning).

Preparation of *A. machipongonensis* conditioned media and isolation of RIF-OMVs

Outer membrane vesicles were isolated from *A. machipongonensis* as described in (89). Briefly, *A. machipongonensis* (ATCC BAA-2233, (111)) was grown in 500 mL 100% SWC, shaking at 30ºC for 48 hours. The bacteria were pelleted and the supernatant was filtered through a 0.2 µm filter to produce conditioned media. Conditioned media was then centrifuged at 36,000 × g for 3 hours at 4ºC (Type 45 Ti rotor, Beckman Coulter). OMV-containing pellets were resuspended in 2 mL ASW.

HPLC purification of RIFs

RIFs were purified by HPLC as described in (89). Briefly, *A. machipongonensis* was grown in 20 L Marine Broth media (Carl Roth (CP.73): 40.1 g/L), shaking at 30ºC for 48 hours. The cells were harvested by centrifugation and extracted with $CHCl_3$:MeOH (2:1, 4L). The organic extract was filtered and concentrated to give approximately 3g crude lipid extract. The crude extract was dissolved in 60% MeOH (+0.1% NH_4OH) and fractionated using a C18-SPE (Solid Phase Extraction) using a 10% step-gradient of MeOH (60%-100% MeOH+0.1 NH_4OH). The resulting SPE fractions were analyzed for sulfonolipid-specific signals using LC-MS and ^{1}H-NMR. The fraction containing RIF-mix (RIF-1 and RIF-2) eluted with 90% MeOH (+0.1% NH_4OH) during the SPE purification.

Rosette induction

Unless otherwise noted, SrEpac cultures were treated with a 1:1,000 dilution of RIF-OMVs and incubated for 24 hours before imaging or counting. To induce a low level of rosette development in the sensitized rosette induction assay (Fig. 2.2B-D, Fig. 2.3B, Fig. 2S2B-D), SrEpac cultures were treated with a 1:20,000 dilution of RIF-OMVs. HPLC-purified RIFs were resuspended in DMSO and added at 10 µg/mL (Fig. 2.3A).

Swarm induction

Unless otherwise noted, cultures were treated with 0.05 U/mL chondroitinase ABC from *P. vulgaris* (Sigma), referred to as "EroS$_{Pv}$". EroS from *V. fischeri* (EroS$_{Vf}$; Fig. 2.3B) was purified as described in (87). Briefly, *V. fischeri* ES114 (ATCC 700601) was grown in 8 L 100% SWC, shaking at 20ºC for 30 hours. The bacteria were

pelleted and the supernatant was filtered through a 0.2 μm filter, concentrated to 120 mL using a using a tangential flow filtration device with a 30 kDa Centramate filter (Pall #OS030T12), then ammonium sulfate precipitated and further separated by size exclusion chromatography. EroS_{Vf} was added to SrEpac cultures at a final dilution of 0.1%.

Rosette quantification

To quantify the percentage of cells in rosettes, cultures were fixed with 1% formaldehyde, vortexed, mounted on a Bright-Line hemacytometer (Hausser Scientific), and counted on a Leica DMI6000B inverted compound microscope. Rosettes were defined as groups of four or more cells, and were distinguished from swarms based on their resistance to mechanical shear and their stereotypical orientation with their basal poles pointed inwards and their flagella out (104, 106). The numbers of solitary cells and rosettes, as well as the number of cells in each rosette, were counted until at least 200 cells were scored (per biological replicate).

Swarm quantification

Cell cluster areas were quantified as described in (87). Briefly, samples were imaged in 96-well glass-bottomed plates (Ibidi 89621) at 10× magnification using transmitted light (bright field) on a Zeiss Axio Observer.Z1/7 Widefield microscope with a Hammatsu Orca-Flash 4.0 LT CMOS Digital Camera. Images were processed and analyzed in ImageJ as follows: 'Smooth' to reduce bacterial background, 'Find Edges' to further highlight choanoflagellate cells, 'Make Binary' to convert to black and white, 'Close-' to fill in small holes, and 'Analyze Particles' to calculate the area of each cell cluster. Particles smaller than 10 μm^2 were removed to reduce background bacterial signal.

Acknowledgements

This material is based upon work originally supported by the National Institutes of Health (R01-GM099533 to N.K.). We thank members of the King lab for critical feedback, especially David Booth, Thibaut Brunet and Ben Larson. We thank Christine Beemelmanns and Chia-Chi Peng for providing HPLC-purified RIFs, Zoe Vernon and Olivia Angiuli for statistics consultation, and Debbie Maizels for help with illustrations in Fig. 2.4.

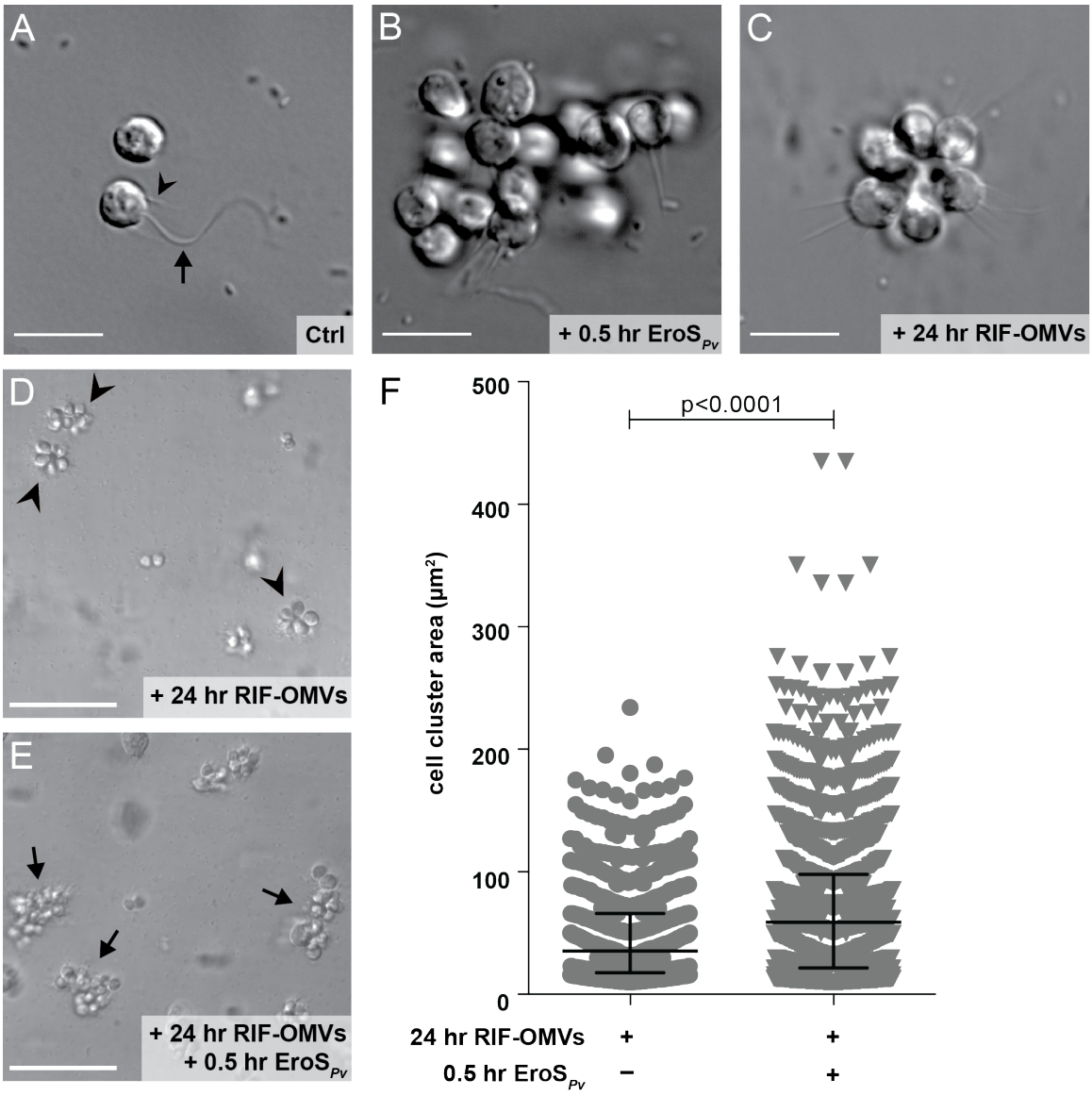

Figure 2.1: Rosettes swarm in response to the EroS$_{Pv}$ mating factor
(A-C) Bacterial cues regulate mating and multicellularity in *S. rosetta*. Scale bars = 10 µm. (A) *S. rosetta* grown in the presence of the prey bacterium *E. pacifica* ("Ctrl") proliferated as solitary cells. This culture served as the foundation for all experiments in this study. A typical *S. rosetta* cell has an apical collar (arrowhead) surrounding a single flagellum (arrow). (B) *S. rosetta* formed mating swarms within 0.5 hours of treatment with the bacterially-produced chondroitinase EroS$_{Pv}$. (C) *S. rosetta* solitary cells developed into rosettes through serial rounds of cell division within 24 hours of treatment with RIF-OMVs from the bacterium *A. machipongonensis*. (D-E) Rosettes swarm in the presence, but not in the absence, of EroS$_{Pv}$. Scale bars = 50 µm. (D) After 24 hours of treatment with RIF-OMVs, solitary cells in an SrEpac culture developed into rosettes (arrowheads) but did not swarm.

(E) Swarms of rosettes (arrows) formed after 24 hours of treatment with RIF-OMVs followed by 0.5 hours of treatment with EroS$_{Pv}$. (F) Shown are the surface areas of cell clusters from SrEpac cultures treated with RIF-OMVs for 24 hours followed by 0.5 hours of incubation either with or without EroS$_{Pv}$. Following the approach of (87), we generated a binary mask to measure cell cluster area (the area of each cell, rosette, or swarm; Fig. 2S1). EroS$_{Pv}$ treatment resulted in clusters of cells, including swarms of rosettes (median = 58.7 μm^2, interquartile range = 21.6-98.0 μm^2), whose areas were significantly larger than those measured in the rosette-only control (median = 35.5 μm^2, interquartile range = 17.8-65.9 μm^2) (Kolmogorov-Smirnov test). 875 cell cluster areas were plotted for the cultures treated with RIF-OMVs and 1359 cell cluster areas were plotted for the cultures treated with RIF-OMVs + EroS$_{Pv}$.

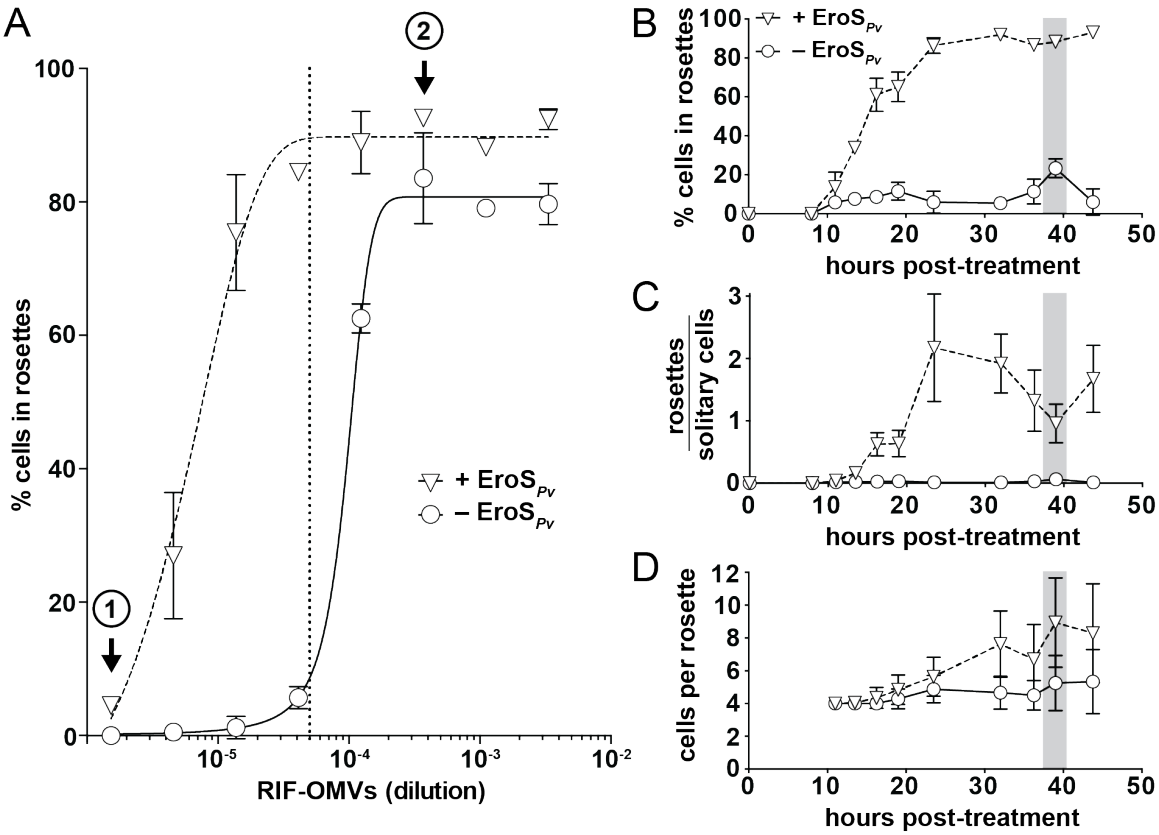

Figure 2.2: The mating inducer EroS$_{Pv}$ enhances rosette development
(A) EroS$_{Pv}$ enhances rosette induction by RIF-OMVs. Treatment of SrEpac with increasing concentrations of RIF-OMVs (circles) resulted in a concomitant increase in the percentage of cells in rosettes. Co-treatment of SrEpac with RIF-OMVs and 0.05 U/mL EroS$_{Pv}$ (triangles) resulted in rosette development at concentrations of RIF-OMVs that did not otherwise induce rosettes (e.g. at (**1**)). EroS$_{Pv}$ also increased the maximum percentage of cells in rosettes at saturating concentrations of RIF-OMVs (e.g. at (**2**)). The 1:20,000 dilution of RIF-OMVs used for the sensitized rosette induction assays in panels B-D is indicated with a vertical dotted line. Mean plotted ± S.D. (B) Co-treatment of SrEpac with EroS$_{Pv}$ and RIF-OMVs leads to a dramatic increase in percentage of cells in rosettes throughout the course of rosette development relative to SrEpac treated only with RIF-OMVs. After 39 hours (shaded bar) of co-treatment with RIF-OMVs and EroS$_{Pv}$ (triangles), 88.2±2.7% (mean ± S.D.) of *S. rosetta* cells were in rosettes, compared with 23.4±4.9% (mean ± S.D.) of cells treated with RIF-OMVs alone (circles). (C) EroS$_{Pv}$ increased the ratio of rosettes to solitary cells in SrEpac cultures treated with RIF-OMVs. After 39 hours (shaded bar) of co-treatment with RIF-OMVs and EroS$_{Pv}$ (triangles), the ratio of rosettes to solitary cells was 0.96±0.31 (mean ± S.D.), compared with 0.06±0.02 (mean ± S.D.) after treatment with RIF-OMVs alone (circles). (D) EroS$_{Pv}$ increased the number of cells per rosette in RIF-OMV-treated SrEpac cultures. After 39 hours (shaded bar) of co-treatment with RIF-OMVs and EroS$_{Pv}$ (triangles), there were 8.9±2.7 (mean ±

S.D.) *S. rosetta* cells per rosette colony, compared with 5.3±1.7 (mean ± S.D.) cells per rosette colony after treatment with RIF-OMVs alone (circles).

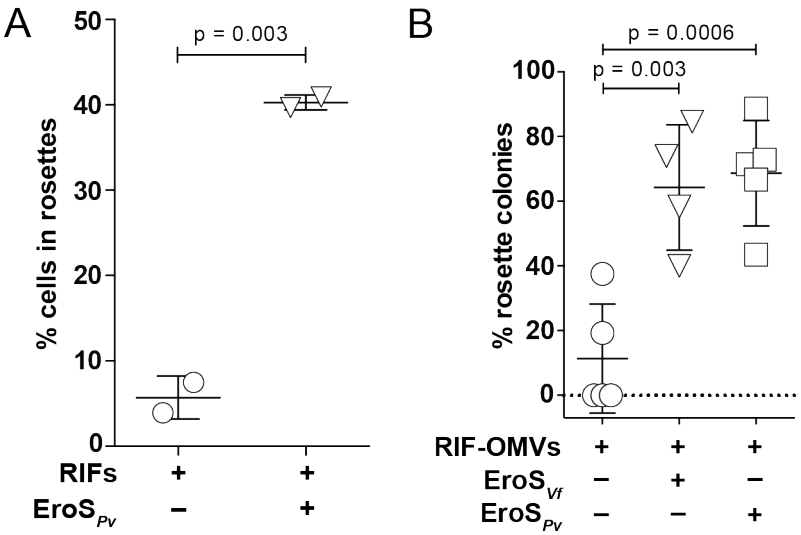

Figure 2.3: Purified RIFs and EroS are sufficient for enhancement of rosette induction

(A) Co-treatment of SrEpac with 10 µg/mL HPLC-purified RIFs and 0.05 U/mL EroS$_{Pv}$ (triangles) resulted in an increase in the percentage of *S. rosetta* cells in rosettes compared to treatment with HPLC-purified RIFs alone (circles). Mean plotted ± S.D. (unpaired *t* test). (B) Co-treatment of SrEpac with a 1:20,000 dilution of RIF-OMVs and either 0.1% EroS from *V. fischeri* (EroS$_{Vf}$), or 0.05 U/mL EroS from *P. vulgaris* (EroS$_{Pv}$) resulted in an increase in the percentage of rosette colonies compared to treatment with RIF-OMVs alone. Mean plotted ± S.D. (unpaired *t* test).

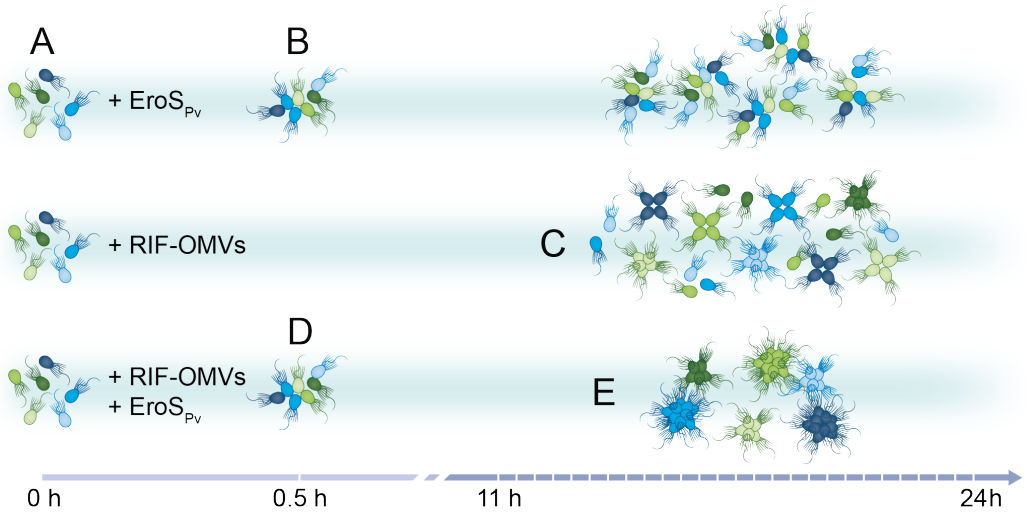

Figure 2.4: *S. rosetta* integration of bacterial cues
S. rosetta phenotypes induced over time by EroS$_{Pv}$, RIF-OMVs, and the synergistic effect of both cues. (A) Untreated SrEpac proliferates as solitary cells. (B) Treatment with EroS$_{Pv}$ induces swarming of unrelated cells within 0.5 hours. (C) Treatment with RIF-OMVs induces rosette development through cell division within 11-24 hours. (D) Co-treatment with RIF-OMVs and EroS$_{Pv}$ for 0.5 hours results in swarming, showing that RIF-OMVs do not interfere with or enhance the activity of EroS$_{Pv}$. (E) After 11-24 hours of co-treatment with RIF-OMVs and EroS$_{Pv}$, rosettes develop and swarm. Compared to treatment with RIF-OMVs alone, co-treatment with RIF-OMVs and EroS$_{Pv}$ induces the development of more rosettes and rosettes containing more cells.

Table 2.1: *S. rosetta* phenotypes induced by EroS$_{Pv}$ and RIF-OMVs

Bacterial cue	Hours after induction	*S. rosetta* phenotype	Effect on swarming	Effect on rosette development
EroS$_{Pv}$	0.5	swarming	induces	n/a
RIF-OMVs	0.5	solitary	none	n/a
EroS$_{Pv}$ + RIF-OMVs	0.5	swarming	induces	n/a
EroS$_{Pv}$	24	swarming	induces	none
RIF-OMVs	24	rosette	none	induces
EroS$_{Pv}$ + RIF-OMVs	24	rosette + swarming	induces	enhances

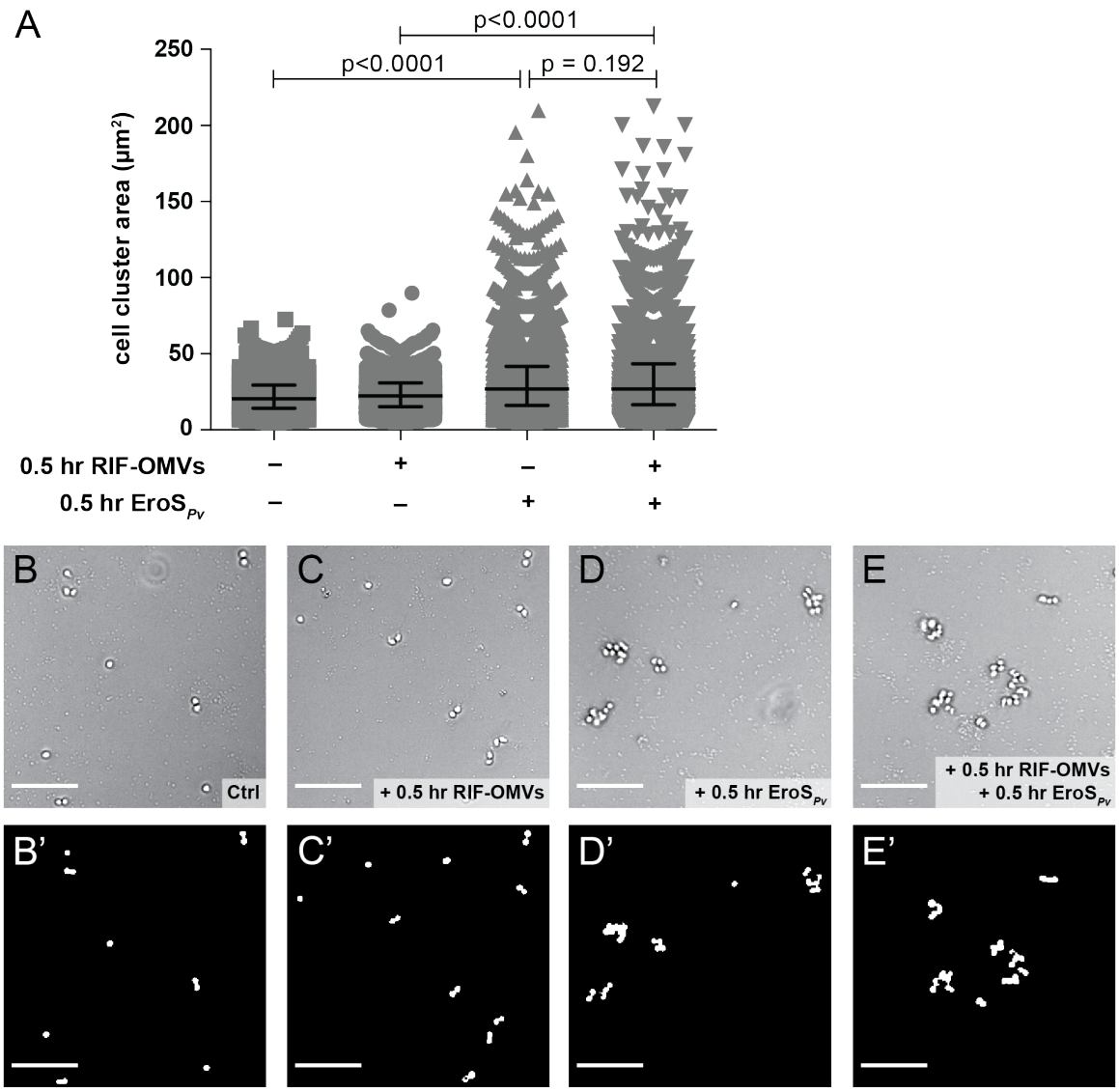

Figure 2S1: RIF-OMVs have no effect on EroS$_{Pv}$-induced swarming
(A) Solitary cells from SrEpac co-treated with RIF-OMVs and EroS$_{Pv}$ formed swarms, quantifiable by an increase in cell cluster area (median = 27.0 μm^2, interquartile range = 16.5-43.5 μm^2) compared to cells treated with RIF-OMVs alone (median = 22.4 μm^2, interquartile range = 15.2-30.8 μm^2). There was no significant difference in swarm size between cells co-treated with RIF-OMVs and EroS$_{Pv}$ and cells treated with EroS$_{Pv}$ alone (median = 27.0 μm^2, interquartile range = 16.0-41.8 μm^2) (Kolmogorov-Smirnov test). A minimum of 2730 cell cluster areas were plotted for each condition. (B-E') Sample images used for quantification in (A). Following the approach of (87), raw images in (B-E) were converted to binary images (B'-E') to measure cell cluster size (Materials and Methods). (B) *S. rosetta* cells from untreated SrEpac remained solitary. (C) *S. rosetta* cells from SrEpac treated with RIF-OMVs for 0.5 hours remained solitary. (D) *S. rosetta* cells from SrEpac treated with EroS$_{Pv}$ for 0.5 hours formed visible swarms. (E) *S. rosetta* cells from SrEpac co-treated with RIF-OMVs and EroS$_{Pv}$ for 0.5 hours formed visible swarms.

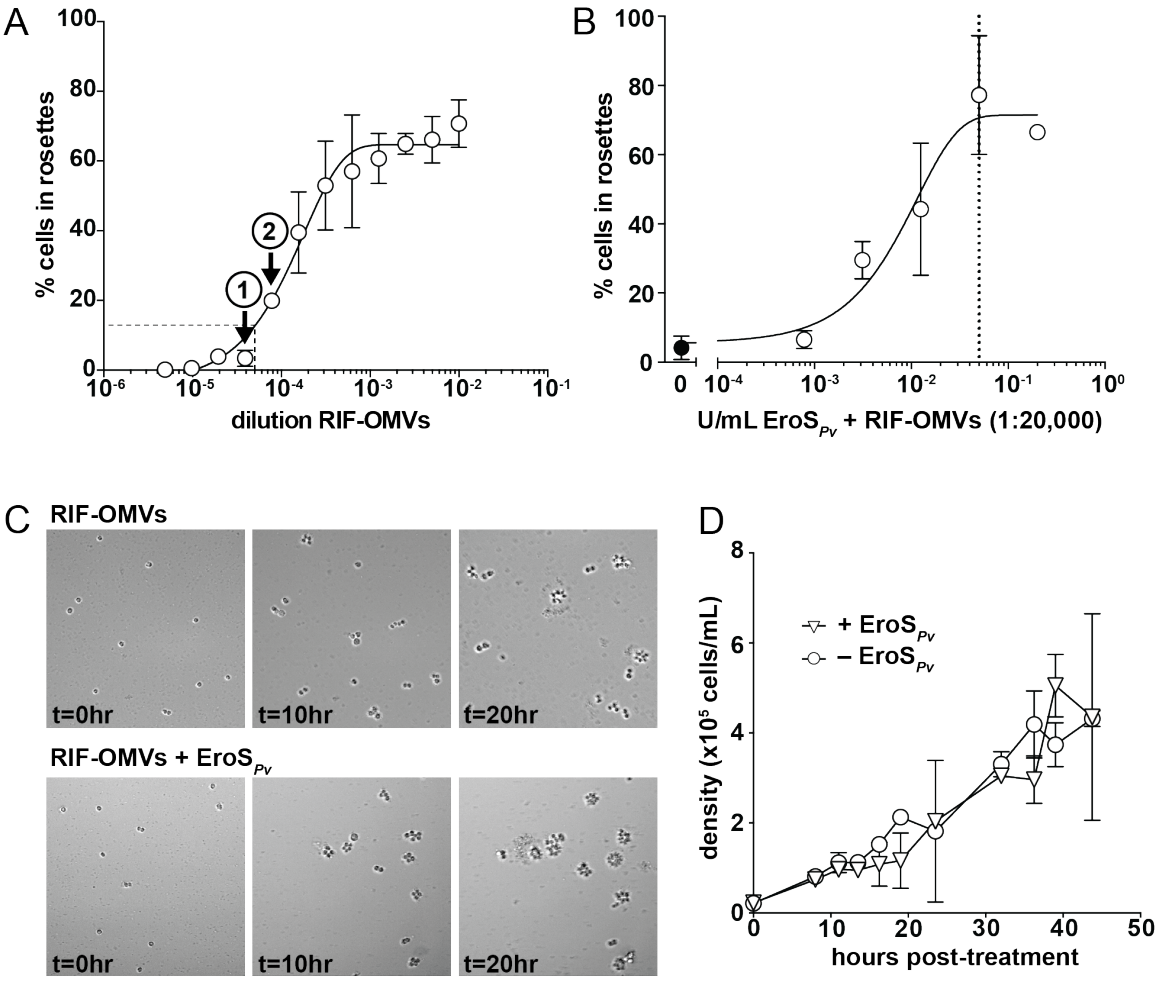

Figure 2S2: EroS$_{Pv}$ enhances rosette development, but not cell proliferation, in a sensitized rosette induction assay

(A) Serial dilution of RIF-OMVs can be used to induce a low percentage of cells in rosettes. SrEpac treated with a 1:25,600 dilution of RIF-OMVs resulted in 3.4±2.3 (mean ± S.D.) *S. rosetta* cells in rosettes (arrow marked (**1**)), while a 1:12,800 dilution of RIF-OMVs resulted in 19.9±1.7 (mean ± S.D.) *S. rosetta* cells in rosettes (arrow marked (**2**)). An intermediate dilution of 1:20,000 was used for the sensitized rosette induction assay (dashed lines). (B) Rosette-enhancing activity correlated with EroS$_{Pv}$ concentration. SrEpac treated with a 1:20,000 dilution of RIF-OMVs (black circle) contained more *S. rosetta* cells in rosettes upon the addition of increasing concentrations of EroS$_{Pv}$ (white circles). Dotted line indicates concentration of EroS$_{Pv}$ (0.05 U/mL) used for subsequent assays. Mean plotted ± S.D. (C) Time-lapse imaging showed an increase in both the number of rosettes and the number of cells per rosette after co-treatment with a 1:20,000 dilution of RIF-OMVs and 0.05 U/mL EroS$_{Pv}$ (bottom) compared to RIF-OMVs alone (top). (D) *S. rosetta* cells treated with RIF-OMVs (circles) or co-treated with RIF-OMVs and EroS$_{Pv}$ (triangles) grew at the same rate. Mean density plotted ± S.D.

Appendix 1

Preliminary findings on the mechanisms by which EroS enhances rosette development

Abstract

As described in Chapter 2, I discovered that the choanoflagellate *Salpingoeca rosetta* integrates distinct bacterial cues (swarm-inducing EroS$_{Pv}$ and rosette-inducing RIFs) to enhance multicellular rosette development. Following up on these results, I sought to uncover the mechanistic basis for the synergy between swarm-inducing and rosette-inducing cues. I discovered that in addition to enhancing the rosette development induced by RIFs, EroS$_{Pv}$ also enhances rosette development induced by other bacterial cues. Furthermore, EroS$_{Pv}$ enhances rosette development in genetic mutants of *S. rosetta* that form rosettes at reduced levels. Taken together, these results suggest that EroS$_{Pv}$ enhancement of multicellularity may not be specific to a single *S. rosetta* target. Additionally, I discovered that EroS$_{Pv}$ treatment results in basal staining for the C-type lectin Rosetteless, a phenotype that had previously only been observed after treatment with RIFs, suggesting a point of convergence for these two pathways.

Introduction

The choanoflagellate *Salpingoeca rosetta* undergoes distinct life history transitions in response to bacterial cues. A bacterial chondroitinase called EroS, which is secreted by *Vibrio fischeri*, *Proteus vulgaris* and select other Gammaproteobacteria, induces solitary *S. rosetta* cells to form mating swarms, which eventually resolve into pairs of cells that fuse and undergo meiotic recombination (87). In contrast, sulfonolipid Rosette Inducing Factors (RIFs), produced by the bacterium *Algoriphagus machipongonensis*, induce solitary *S. rosetta* cells to undergo serial rounds of cell division without separation, resulting in the development of multicellular rosettes of cells that are physically linked by cytoplasmic bridges and a shared extracellular matrix (88, 89, 104, 105). Surprisingly, I found that *S. rosetta* is able to integrate the bacterial swarm-inducing and rosette-inducing cues to enhance multicellular development, resulting in both larger rosette colonies and an increase in the number of colonies (Chapter 2).

Because the *S. rosetta* targets of these bacterial cues are as-yet unknown, I was unable to directly test how each bacterial cue interacts with the other cue's target. However, I did have several other tools at my disposal for investigating the nature of this interaction. First, in addition to *A. machipongonensis*, other diverse species of bacteria, including the mucin-degrading intestinal commensal *Akkermansia muciniphila* and the Gram-positive marine bacterium *Demequina spp*., induce rosette development (94). These bacteria are not known to produce sulfonolipids, which, in bacteria, thus far have only been described in Bacteroidetes (e.g. (88, 118–120)). I therefore hypothesized that these different bacteria induce rosette development through the use of chemically and structurally distinct molecules. Rosette induction by *A. machipongonensis* RIFs is believed to be receptor-mediated because rosette induction is dose-responsive, RIFs are highly potent (active at femtomolar concentrations) and RIF activity can be inhibited by a similarly structured lipid, Inhibitor of Rosettes (IOR) (88, 89, 91). Furthermore, RIF activity has stringent structural requirements, indicative of a highly specific receptor-ligand interaction (88–90). Therefore, the rosette-inducing molecules produced by *A. machipongonensis*, *A. muciniphila* and *Demequina spp.* may target distinct *S. rosetta* receptors.

I also took advantage of a set of *S. rosetta* "Class B" mutants that form rosettes in response to *A. machipongonensis* RIFs, but do so at a reduced level compared to wild type (106, 121). Although their underlying genetic mutations are unknown, the reduced rosette development phenotype served as a useful tool to test whether EroS could enhance rosette development in different genetic backgrounds.

Finally, I investigated whether the EroS and RIF-induced pathways converge on the extracellular matrix (ECM). The composition of the *S. rosetta* extracellular matrix has not yet been characterized, but the *S. rosetta* genome encodes homologs of animal ECM proteins and protein domains, including C-type lectins and collagen repeats (122) and the proteins required to synthesize chondroitin sulfate (87). The ECM plays an essential role in rosette development in *S. rosetta*. An ongoing genetic screen has revealed that proper expression and basal secretion of the C-type lectin Rosetteless (Rtls; (106)) and the activities of two putative glycosyltransferases

(121) are essential for proper rosette development. Notably, perturbing the stiffness of the *S. rosetta* ECM during rosette development disrupts rosette morphology (110). *S. rosetta* ECM also mediates mating. EroS degrades chondroitin sulfate, a component of proteoglycans in the ECM of animals (123) and *S. rosetta* (87). I therefore hypothesized that modification of the ECM by the chondroitin lyase activity of EroS might enhance rosette development.

Results

EroS$_{Pv}$ broadly enhances rosette development in *S. rosetta*

I used a culture containing *S. rosetta* and the prey bacterium *Echinicola pacifica* (together comprising a culture called SrEpac; (106, 107)), as the basis for these experiments. In SrEpac, solitary *S. rosetta* cells proliferated rapidly, but underwent no other observable cell state transitions.

To determine whether EroS can enhance rosette development induced by different species of bacteria, I treated SrEpac cultures with different bacterial rosette-inducing cues: RIFs contained in outer membrane vesicles (OMVs) from *A. machipongonensis* (*Alg*), OMVs from *A. muciniphila* (*Akk*), or conditioned media from *Demequina spp.* (*Dem*). I found that co-treatment with EroS from *P. vulgaris* (EroS$_{Pv}$) increased the percentage of cells in rosettes induced by all three bacteria (Fig. A1.1A). This result suggests that EroS$_{Pv}$ rosette enhancement does not require RIFs or an *S. rosetta* receptor that is specific to RIFs.

To further investigate where EroS acts in the rosette induction pathway, I tested whether EroS$_{Pv}$ also enhances rosette development in mutants of *S. rosetta* – Slacker, Uptight and M17C12 – that form rosettes at reduced levels compared to wild type (106, 121). *S. rosetta* mutants were treated for 24 hours with a 1:1,000 dilution of *A. machipongonensis* RIF-OMVs (to induce the maximum rosette levels in the mutant strains) alone or in combination with EroS$_{Pv}$. EroS$_{Pv}$ increased the percentage of cells in rosettes in all of the mutants, in addition to the wild type *S. rosetta* control (SrEpac, which was treated with a 1:20,000 dilution RIF-OMVs to induce rosette development in a small percentage of the population and allow sensitive detection of enhancement) (Fig. A1.1B). Although the causative mutations underlying reduced rosette development in these mutants are unknown, these data provide further evidence that EroS$_{Pv}$ may enhance rosette development through a generic stage of the rosette development pathway.

EroS$_{Pv}$ induces basal Rtls staining

In rosettes, Rtls protein is secreted from the basal pole of each cell into the central ECM, while in the majority of non-rosette cells Rtls protein is detectable only at low levels and is retained in the subcortical region of the basal cell pole (106). To determine whether EroS$_{Pv}$ influences the localization of Rtls in non-rosette cells, I treated SrEpac cells with EroS$_{Pv}$ for 0.5 hours and immunostained for Rtls and tubulin (to mark the cell body and flagellum). As previously shown by Levin et al., Rtls was only rarely detected (in 2.0±0.9% of cells) at the basal poles of untreated non-rosette cells (Fig. A1.2A, C) (106). In EroS$_{Pv}$-treated samples, however, Rtls staining was detected at the basal pole of 10.9±2.7% of cells (Fig. A1.2B, C), despite

the fact that the cells had not been treated with RIFs and did not develop into rosettes. By quantifying the intensity of Rtls staining along the apical-basal axis in all imaged cells, I found an increase in Rtls fluorescence intensity specifically at the basal poles of EroS$_{Pv}$-treated cells relative to untreated cells (Fig. A1.2D). Therefore, EroS$_{Pv}$ treatment triggers an increase in the quantity of Rtls detectable at the basal pole of *S. rosetta* cells, which had previously only been observed during rosette development. For technical reasons, I was unable to compare EroS$_{Pv}$ treatment to treatment with RIF-OMVs or co-treatment with RIF-OMVs and EroS$_{Pv}$, or study the effect of treatment over the 11-24 hour period required for rosette development. Interestingly, although basal Rtls staining was observed in EroS$_{Pv}$-treated cells, Rtls was not required for swarming (Fig. A1.3A-E).

Discussion

Chondroitin sulfate modification can occur on a wide range of proteoglycans, and its digestion can regulate proteoglycan function. Because Eros$_{Pv}$ increased the sensitivity of *S. rosett*a not only to the sulfonolipid RIFs, but also to non-RIF rosette-inducing cues from diverse bacteria (Fig. A1.1A), which likely target different receptors, I hypothesize that EroS may modify chondroitin sulfate moieties on multiple proteoglycan receptors or co-receptors for rosette-inducing cues. Enzymatic digestion of glycans on growth factor receptors has been shown to enhance ligand-mediated receptor activation (108), and proteoglycan co-receptors can further enhance receptor function by stabilizing or sequestering ligands (124, 125). Alternatively, the target of EroS may not be a receptor, but a different *S. rosetta* protein in the rosette-development pathway that is shared between the different bacterial cues. Future research aimed at determining the *S. rosetta* targets of EroS will reveal more about whether they might function as receptors or co-receptors for rosette-inducing molecules.

One component of the ECM of rosettes, the C-type lectin Rtls, is essential for rosette development. Surprisingly, EroS$_{Pv}$ treatment results in an increase in the quantity of Rtls detectable at the basal pole of *S. rosetta* cells (Fig. A1.2), which had previously only been observed during rosette development. This may indicate that EroS induces relocalization of Rtls to the basal cytoplasm of the cell, or basal secretion of Rtls. Future experiments comparing permeabilized and unpermeabilized cells will help determine whether Rtls is secreted in response to EroS treatment. Alternatively, Rtls may already be present at the basal pole, buried beneath the ECM, and be revealed by EroS digestion of the ECM. If this were the case, I would expect treatment with other enzymes that digest the ECM to also expose the Rtls epitope.

The presence of basal Rtls is not sufficient for rosette development, as EroS$_{Pv}$ treatment alone does not induce rosettes. Comparison of cells co-treated with RIF-OMVs and EroS$_{Pv}$ may reveal whether EroS increases the amount of Rtls secreted during rosette development, which would support a role for Rtls secretion in rosette enhancement (in addition to being required for rosette development). During EroS-induced mating, cells fuse at their basal poles (87), further indicating that

remodeling of this region by EroS may influence both mating and rosette development.

Materials and Methods

Choanoflagellate culturing conditions

Artificial seawater (ASW) was prepared by diluting 32.9 g Tropic Marin sea salts in 1L water for a salinity of 32-37 parts per thousand (107). Sea Water Complete media (SWC) was prepared by diluting 5 g/L peptone, 3 g/L yeast extract, and 3 mL/L glycerol in ASW (107). SrEpac (*Salpingoeca rosetta* co-cultured with the prey bacterium *Echinicola pacifica*, ATCC PRA-390; (107)) and SrEpac mutant strains (Fig. A1.1B, Fig. A1.3) were cultured in 5% Sea Water Complete media (5% SWC vol/vol in ASW) at 22ºC. Cultures were passaged daily, 1 mL into 9 mL fresh media in 25cm^2 cell culture flasks (Corning). Prior to rosette or swarm induction, cultures were diluted to 1×10^5 choanoflagellate cells/mL in 5% SWC and 100 µL volumes were aliquoted into a 96-well plate (Corning).

Preparation of bacterial conditioned media and isolation of OMVs

A. machipongongensis (ATCC BAA-2233, (111)) and *Demequina spp.* (94) were grown in 500 mL 100% SWC, shaking at 30ºC for 48 hours. *A. muciniphila* (ATCC BAA-835, (126)) was grown in 500 mL Brain Heart Infusion broth (37 g/L, Sigma) under anaerobic conditions for 7 days. The bacteria were pelleted and the supernatant was filtered through a 0.2 µm filter to produce conditioned media. *A. machipongongensis* and *A. muciniphila* OMVs were prepared by centrifuging conditioned media at 36,000 x g for 3 hours at 4ºC (Type 45 Ti rotor, Beckman Coulter). OMV-containing pellets were resuspended in 2 mL ASW.

Rosette induction and quantification

Unless otherwise noted, SrEpac cultures were treated with a 1:20,000 dilution RIF-OMVs and incubated for 24 hours before counting. To compare inducing cues from different species of bacteria (Fig. A1.1A), cultures were treated with a 1:10,000 dilution *A. machipongonensis* OMVs (*Alg*), a 1:10,000 dilution *A. muciniphila* OMVs (ATCC BAA-835; *Akk*), or 10% conditioned media from *Demequina spp.* (environmental isolate; *Dem*). Class B mutant SrEpac strains were treated with a 1:1,000 dilution RIF-OMVs (Fig. A1.1B).

To quantify the percentage of cells in rosettes, cultures were fixed with 1% formaldehyde, vortexed, mounted on a Bright-Line hemacytometer (Hausser Scientific), and counted on a Leica DMI6000B inverted compound microscope. Rosettes were defined as groups of four or more cells, and were distinguished from swarms based on their resistance to mechanical shear and their stereotypical orientation with their basal poles pointed inwards and their flagella out (104, 106). The numbers of solitary cells and rosettes, as well as the number of cells in each rosette, were counted until at least 200 cells were scored (per biological replicate).

Swarm induction and quantification

Cultures were treated with 0.05 U/mL chondroitinase ABC from *P. vulgaris* (Sigma), referred to as "EroS_{Pv}".

Cell cluster areas (Fig. A1.3) were quantified as described in (87). Briefly, samples were imaged in 96-well glass-bottomed plates (Ibidi 89621) at 10× magnification

using transmitted light (bright field) on a Zeiss Axio Observer.Z1/7 Widefield microscope with a Hammatsu Orca-Flash 4.0 LT CMOS Digital Camera. Images were processed and analyzed in ImageJ as follows: 'Smooth' to reduce bacterial background, 'Find Edges' to further highlight choanoflagellate cells, 'Make Binary' to convert to black and white, 'Close-' to fill in small holes, and 'Analyze Particles' to calculate the area of each cell cluster. Particles smaller than 10 μm^2 were removed to reduce background bacterial signal.

Immunofluorescence microscopy

Immunostaining (Fig. A1.2A-B) was performed previously described by (106). Briefly, cells were allowed to settle on poly-L-lysine coated coverslips, then fixed in 6% acetone for 5 min followed by 4% paraformaldehyde for 15 min. Cells were stained with anti-Rosetteless (1:500, (106)), E7 anti-tubulin (1:500, Developmental Studies Hybridoma Bank), Alexa fluor 647 anti-mouse and Alexa fluor 488 anti-rabbit (1:500 each, Molecular Probes), then mounted on ProLong Diamond Antifade Mountant (Molecular Probes). Samples were imaged on a Zeiss Axio Observer.Z1/7 Widefield microscope with a Hamamatsu Orca-Flash 4.0 LT CMOS Digital Camera and a 63x/NA1.40 Plan-Apochromatic oil immersion objective. For confocal images, samples were imaged on a Zeiss Axio Observer LSM 880 with a 63x/NA1.40 Plan-Apochromatic oil immersion objective. Confocal stacks were acquired using the following settings: 35 x 35 nm pixel size, 47 nm z-step, 0.7-1.54 µsec/pixel dwell time, 488 laser operating at 0.5% laser power and 533 gain, 633 laser operating at 2% laser power and 550 gain, 458/561/633 nm multiple beam splitter, and 490-615 nm and 638-755 nm bandpass filters.

Quantification of Rosetteless staining

To quantify the percentage of Rtls-positive cells (Fig. A1.2C), Z-stack images were max projected using ImageJ. A fluorescence intensity threshold for the Rtls channel was created based on *rtls*^{l1} mutant staining and applied to all samples. 'Analyze Particles' was used to determine the number of fluorescent cells above the threshold in each image. The total number of cells was calculated in the tubulin channel using 'Make Binary' to convert to black and white and 'Analyze Particles' to count cells (only particles over 10 μm^2 were counted to remove background bacterial signal). At least 663 cells from 2 biological replicates were analyzed per condition.
To quantify Rtls fluorescence intensity along the basal-apical axis (Fig. A1.2D), Z-stack images were max projected using ImageJ. Individual cells were chosen based on the ability to clearly see a cell body and flagellum by tubulin staining. A line was drawn using only the tubulin staining from the point opposite the base of the flagellum to the base of the flagellum, and Rtls fluorescence intensity was measured along the line. To compare between cells, the lines drawn along the cell bodies were one-dimensional interpolated in R to include 150 points and normalized to the length of the line. The average fluorescence intensity was plotted over the length of the basal-apical axis for untreated and EroS$_{Pv}$-treated samples with a 95% confidence interval. Measurements were taken from two biological replicates with at least 50 cells per condition.

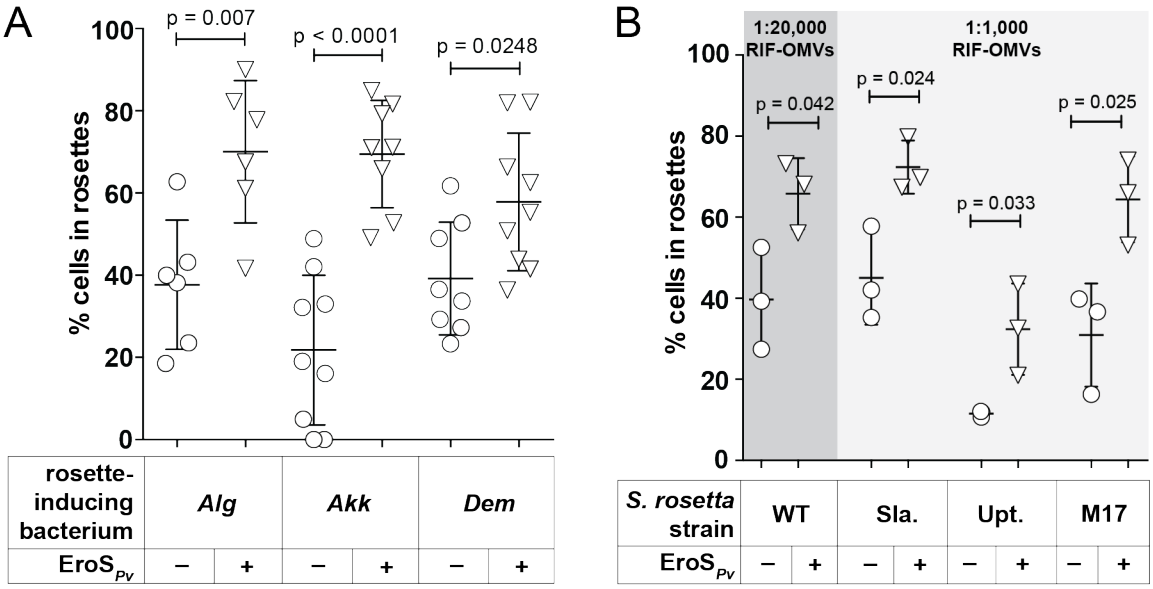

Figure A1.1: EroS$_{Pv}$ broadly enhances rosette development in *S. rosetta*
(A) EroS$_{Pv}$ enhanced rosette induction by distinct bacterial cues. Co-treatment of SrEpac with EroS$_{Pv}$ and RIF-OMVs (*Alg*), *Akkermansia muciniphila* OMVs (*Akk*), or *Demequina spp.* conditioned media (*Dem*) increased the percentage of cells in rosettes compared to *Alg*, *Akk* or *Dem* alone (unpaired *t* test). (D) EroS$_{Pv}$ enhanced rosette development in rosette-defective mutants. Class B mutants, which form reduced levels of rosettes, were treated with RIF-OMVs, with or without 0.05 U/mL EroS$_{Pv}$, for 24 hours. WT=wild type, Sla.=Slacker, Upt.=Uptight, M17=M17C12 (106, 121) (unpaired *t* test).

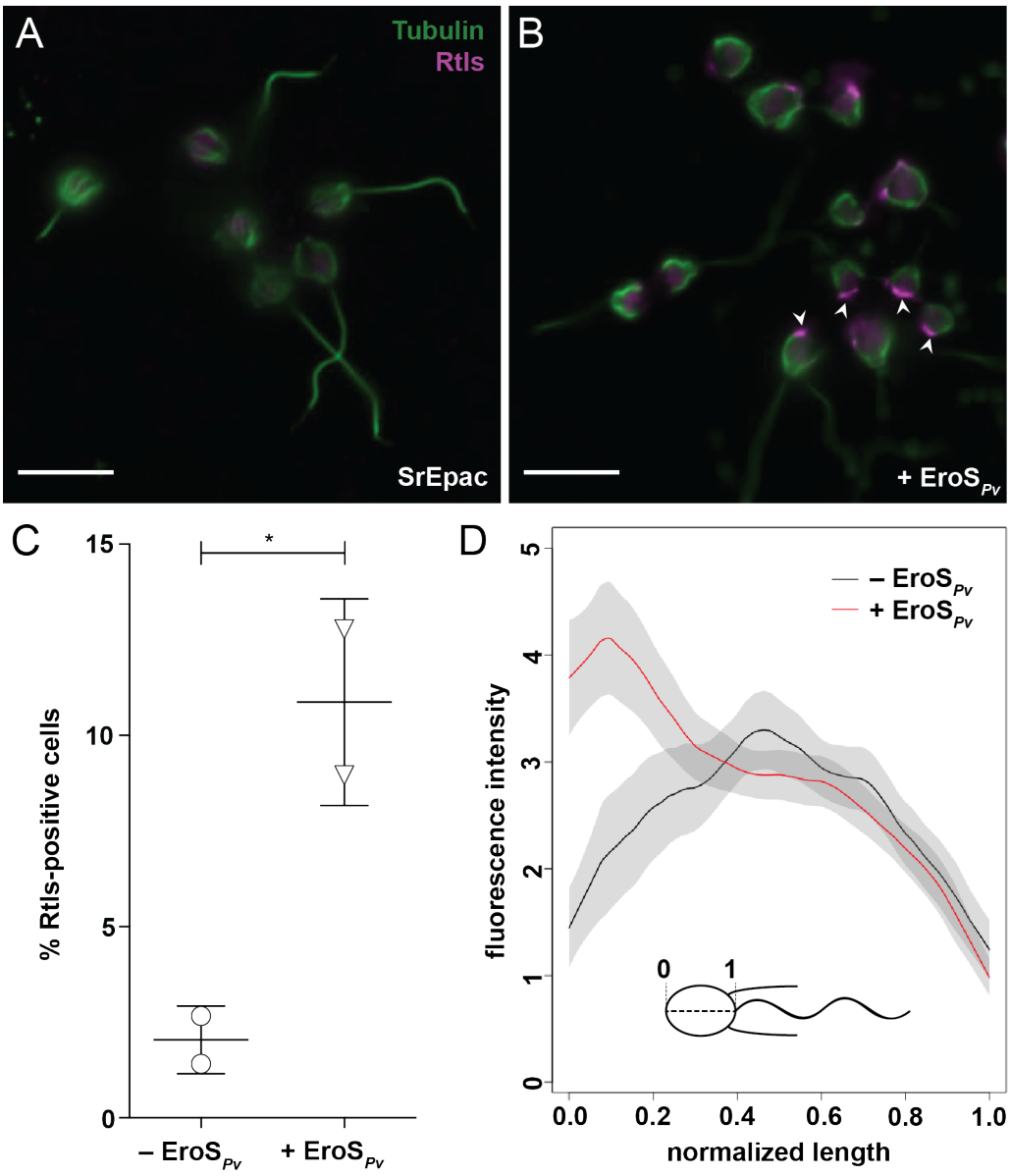

Figure A1.2: EroS$_{Pv}$ induces basal Rtls staining
(A-B) Cells were immunostained with anti-tubulin to visualize the cell body and flagellum (green) and anti-Rtls (magenta). Scale bars = 10 µm. (A) Untreated *S. rosetta* cells showed no basal Rtls staining. (B) *S. rosetta* cells treated with EroS$_{Pv}$ for 0.5 hours before immunostaining showed basal Rtls staining (arrowheads). (C) EroS$_{Pv}$ treatment resulted in an increase in the number of Rtls-positive cells. Fluorescence intensity threshold was set based on *rtls*^{I1} mutant staining and Rtls-positive cells (as in A-B) were counted and divided by the total number of cells. (n ≥ 663 cells per condition, unpaired t test, p = 0.048). (D) Rtls staining was localized to the basal pole of EroS$_{Pv}$-treated, but not untreated, *S. rosetta* cells. Average Rtls fluorescence intensity along the basal-apical axis (as defined by tubulin staining of the cell body, normalized for cell size) was plotted for at least 50 cells per condition. Gray shading indicates 95% confidence intervals.

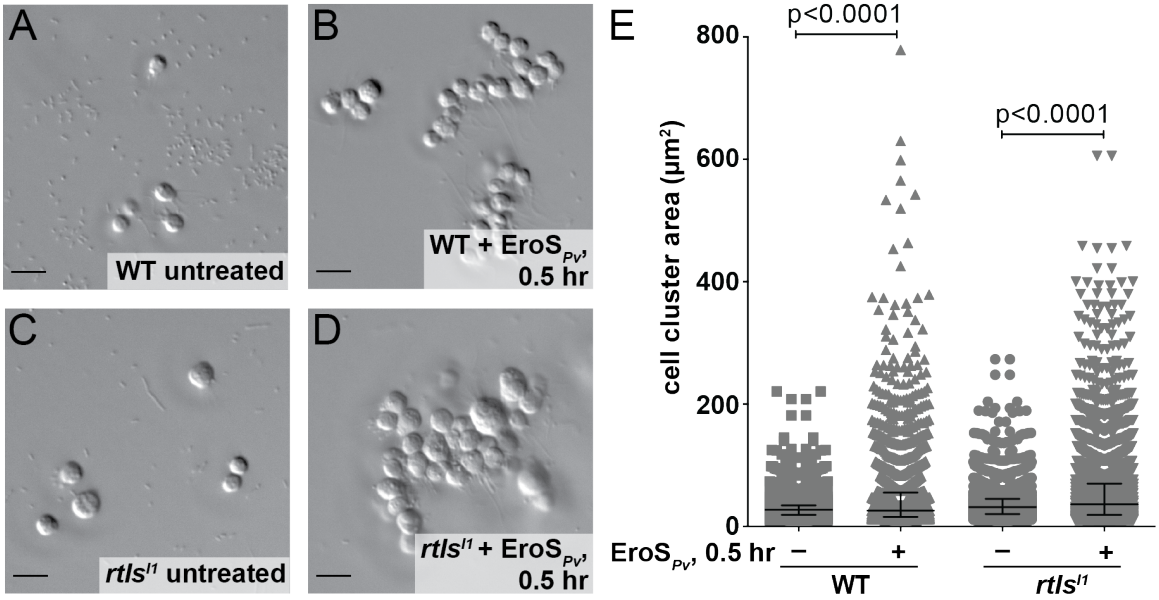

Figure A1.3: Rtls is not required for swarming
(A-D) Scale bars = 10 μm. (A) Untreated wild type (WT) *S. rosetta* did not form swarms. (B) WT S*. rosetta* treated with EroS$_{Pv}$ formed swarms within 0.5 hours. (C) Untreated *rtls*^{l1} mutant (106) did not form swarms. (D) *rtls*^{l1} mutant treated with EroS$_{Pv}$ formed swarms within 0.5 hours. (E) EroS$_{Pv}$-treated WT *S. rosetta* swarms and *rtls*^{l1} mutant swarms were quantifiable by an increase in cell cluster area (WT median = 26.2 μm^2, interquartile range = 15.6-55.4 μm^2; *rtls*^{l1} median = 36.3 μm^2, interquartile range = 19.0-70.1 μm^2) compared to untreated controls (WT median = 27.5 μm^2, interquartile range = 19.0-34.7 μm^2; *rtls*^{l1} median = 31.7 μm^2, interquartile range = 20.3-45.2 μm^2). A minimum of 1976 cell cluster areas were plotted for each condition. (Kolmogorov-Smirnov test).

Appendix 2

Forward genetic screens to identify a rosette-inducing factor (RIF) receptor

Abstract

The choanoflagellate *Salpingoeca rosetta* transitions from a unicellular to a multicellular "rosette" life stage in response to specific sulfonolipids called Rosette Inducing Factors (RIFs) from the bacterium *Algoriphagus machipongonensis*. Forward genetic screens have uncovered some of the *S. rosetta* genes involved in rosette development, but the target(s) of RIFs have not yet been characterized. These screens have been hampered by two major bottlenecks: low rates of mutagenesis, and the time and labor required to screen all phenotypes by eye. I tested new methods of mutagenesis, but was unable to significantly improve upon previous results. I also developed a flow cytometry-based rosette selection method, which was inconsistent but shows potential as a tool for enriching for rosettes. In addition to optimizing screening efficiency, I developed two complementary genetic screens to attempt to identify the target(s) of RIFs, which were unfortunately unsuccessful.

Introduction

Bacterially-induced multicellularity in the choanoflagellate *S. rosetta*

Multicellularity has evolved independently in multiple branches of the tree of life, including in animals and their closest living relatives, the choanoflagellates (127). The transition between a unicellular and multicellular life stage in one choanoflagellate, *Salpingoeca rosetta*, is governed by bacterial cues. Specific bacteria induce solitary cells of *S. rosetta* to develop into multicellular rosette-shaped colonies, through serial cell divisions without complete cytokinesis (88, 104, 105). The inducing molecules from one such bacterium, *Algoriphagus machipongonensis*, have been identified as sulfonolipids called Rosette Inducing Factors (RIFs) (88, 89). However, the *S. rosetta* target(s) of RIFs have yet to be characterized. Here, I used two complementary genetic screens to attempt to identify the target(s) of RIFs.

Bottlenecks to forward genetic screens

Until recently (128), reverse genetic tools were unavailable in *S. rosetta*. Forward genetic screens had been successfully used to link phenotypes to the underlying genes (106, 121), but these screens had two major bottlenecks limiting their efficiency.

First, mutagenesis has only been observed at a low rate after treatment with either the chemical mutagen ethyl methanesulfonate (EMS) or X-rays (106, 121). In a screen for mutants defective in rosette formation, out of 37,269 clones screened, only 16 mutants were identified, a rate of 0.043% (106, 121). In the mutants that were whole-genome resequenced, few validated mutations were identified (106, 121), suggesting a low rate of mutagenesis. *rtls*^{l1}, the first mutant for which the causative gene was mapped, has only four unique genetic markers compared to the reference genome and parental strain (106). While this made it easier to identify the causative mutation (in the case of *rtls*^{l1}, a splice donor mutation in the gene coding for C-type lectin called Rosetteless), the low mutation rate poses a problem when it comes to actually isolating specific mutants of interest.

Second, in addition to low mutagenesis rates, the prior screens for rosette defect mutants were laborious due to the need to screen all phenotypes by eye. Although rosettes and solitary cells can be distinguished by eye, there are few markers that differentially stain rosettes and solitary cells. The clearest marker is a polyclonal antibody against Rosetteless, which stains the ECM of rosettes but does not strongly stain solitary cells. However, the Rosetteless antibody has only been generated once, and is in limited supply. Furthermore, it has not been validated for use in fluorescence-activated cell sorting (FACS) or other selection methods. Therefore, a new method of differentiating between rosettes and solitary cells is needed for a more efficient screening process.

A conditional screen to identify a RIF-receptor

In addition to *A. machipongonensis*, other phylogenetically diverse bacteria, including the mucin-degrading intestinal commensal *Akkermansia muciniphila* and the Gram-positive marine bacterium *Demequina spp*., also induce rosette development in *S. rosetta* (88, 94). However, unlike *A. machipongonensis*, these

bacteria are not known to produce sulfonolipids. It is therefore believed that different bacteria induce rosette development through the use of chemically and structurally distinct molecules.

Rosette induction by *A. machipongonensis* RIFs is believed to be receptor-mediated, because rosette induction is dose-responsive, RIFs are highly potent (active at femtomolar concentrations) and RIF activity can be inhibited by a similarly structured lipid, Inhibitor of Rosettes (IOR) (88, 89, 91). Furthermore, RIF activity has stringent structural requirements, indicative of a highly specific receptor-ligand interaction (88–90).

I therefore hypothesized that different bacteria induce rosette development through distinct *S. rosetta* receptors. If this were true, it should be possible to isolate *S. rosetta* mutants that would respond to cues from one rosette-inducing bacterial species but not another. I called these putative mutants "conditional mutants" because their mutant phenotype is only expressed under specific environmental conditions (in this case, the presence of a particular bacterium).

A constitutive mutant selection to identify a RIF-receptor

In parallel with the conditional mutant screen, I pursued a selection approach to isolate constitutive rosette formation mutants. I hypothesized that even with low mutagenesis rates, I would be able to select for constitutive mutants by repeated rounds of mutagenesis, sensitization of the culture with low levels of rosette-inducing cues, and selection for rosettes. I hypothesized that the selection of rosettes from a large population of cells would allow me to isolate potentially rare constitutive rosette formation mutants that might otherwise be missed.

Results

Optimizing mutagenesis

Before beginning a new set of screens, I sought to improve both mutagenesis and the screening process, to increase the likelihood of isolating a mutant of interest in a timely manner.

To improve upon mutagenesis, I first screened a range of doses of chemical mutagens for reduction of *S. rosetta* cell number, as an indirect measure of mutagenesis. Since mutations in essential genes would be lethal, I inferred that decreasing cell numbers would correlate with increasing mutagenesis rates (although non-specific mutagen toxicity may also contribute to cell death (129)). For this and all following experiments, I used a culture of *S. rosetta* with the prey bacterium *Echinicola pacifica*, together comprising a monoxenic culture called SrEpac.

In previous screens, the relatively low dose of 0.3% EMS (an alkylating agent) was used in order to minimize background mutations that might make mapping causative mutations difficult. This dose resulted in an average of 10% reduction in cell number after 24 hours (Levin). To maximize the efficiency of mutagenesis, I first washed the SrEpac cultures to remove most of the prey bacterium *E. pacifica*, to reduce the likelihood of the bacterium acting as a sponge for the mutagen. I then treated the cultures with up to two-fold higher concentrations of EMS (0.05-5%)

than previously used. I also tested a range of doses of another alkylating agent, *N*-ethyl-*N*-nitrosourea (ENU, 0.5-50 mM). I did not test X-ray mutagenesis, which is more likely to cause large indels and chromosomal rearrangements, because I hypothesized that point mutations and small indels would be more likely to result in one of my phenotypes of interest (a constitutively active rosette pathway). After treatment with either EMS or ENU, I reinoculated the SrEpac cultures with *E. pacifica* from a fresh liquid culture.

I found that after treatment with either EMS or ENU, cell number tended to decrease with increasing doses of mutagen, indicating that the mutagens were effective. Cell death appeared to plateau at 10-50 mM ENU, with an average of 46-59% fewer cells than the control 24 hours after treatment (Fig. A2.1A). For all following experiments I used a 50 mM dose of ENU, which was the highest dose tested that caused a significant decrease in cell number, without causing the cells to lyse and crash out of solution.

To further validate mutagenesis, I resequenced the genomes of clonal isolates that had been treated 4 days prior with 50 mM ENU (as above). To isolate clones, I performed limiting dilution in 96-well plates, at an approximate density of 1 cell per 10 wells. The probability that each isolate underwent a clonal bottleneck during this step was 0.905-0.995, calculated using the Poisson distribution (Levin and King, 2013). To ensure that each isolate was truly clonal, I repeated the clonal isolation, resulting in an overall probability of ≥0.991 that each isolate underwent a clonal bottleneck at least once.

After 5-6 days of growth, I selected 9 clones and expanded them in 100 mL media, then treated the cultures with 20 μg/mL rifampicin to remove the prey bacterium *E. pacifica*. I validated the efficacy of antibiotic treatment by counting both choanoflagellate cells and bacterial colony forming units (CFUs), and found a range between 5.2–308 choanoflagellate cells per bacterial cell after washing (Fig. A2.1B). After pelleting the remaining *S. rosetta* cells from culture, I performed DNA extraction and Illumina library prep. I sequenced each clone, along with the unmutagenized parental strain, on an Illumina HiSeq 2500. Variants were called against the reference genome (122), and background mutations were filtered out by comparison to the unmutagenized parental strain.

After filtering out low-quality reads, I called an average of 19,356 total variants per clone (Fig. A2.1C), or an average mutation frequency of 3.5×10^{-4} variants per base (the *S. rosetta* genome is approximately 55 Mb (122)). The variants consisted of ~2-fold more single nucleotide polymorphisms (SNPs) than insertions or deletions (INDELs) (Fig. A2.1C). A:T>G:C and G:C>A:T transitions made up ~63% of SNPs (Fig. A2.1D). However, I later learned that the number of mutations called in the clones was artificially high because I did not filter out low-coverage variants. Although the average coverage across the genome was 10.28X, the coverage for each variant called ranged from a single read to 2,551 reads. Therefore many of the low-coverage variants called may have been simply sequencing errors, and the actual mutation rate may have not been much higher than background.

Optimizing selection for rosettes

I next sought a method for efficiently sorting rosettes from solitary cells in a mixed population, to facilitate the screen for a constitutive rosette mutant. To do this, I took advantage of the difference in size between solitary cells (~5 μm diameter) and rosettes (which consist of 4-25 cells and can have a diameter >10 μm (110)).

To create a mixed population, I mixed solitary cells from an untreated culture of SrEpac with rosettes from an SrEpac culture that had been treated for 24 hours with a 1:1,000 dilution of outer membrane vesicles from *A. machipongonensis* (which contain the full suite of rosette-inducing lipids and fully recapitulate rosette induction by the live bacteria (89)). First, I attempted size selection by filtering the mixed population through an 8 μm membrane, but this did not yield a significant change in the fraction of rosettes (Fig. A2.2A), potentially because *S. rosetta* cells have a non-rigid cell membrane and might be able to change their shape to squeeze through small openings. I next tested two different centrifugation methods, either centrifuging in culture media at low speeds, or with a Percoll density gradient (Materials and Methods). Neither method consistently separated rosettes from solitary cells (Fig. A2.2B-C). I hypothesized that because *S. rosetta* cells beat their flagella to move within the water column (130, 131), inhibition of flagellar motion may cause rosettes to settle faster than solitary cells, based on their larger size. I therefore treated mixed cultures of rosettes and solitary cells with a dynein inhibitor, visually verified that it stopped flagellar motion, and allowed cells to settle passively. However, this method was also unsuccessful at separating rosettes from solitary cells (Fig. A2.2D).

Finally, I tested whether rosettes and solitary cells could be separated based on their forward scatter (an approximation of size) and side scatter (an approximation of granularity) on a flow cytometer. By comparing a mostly-rosette culture to a solitary-celled culture, I was able to see a distinct shift in both parameters (Fig. A2.2E). I set gates for both the solitary-celled (S) and rosette (R) populations and used the R gate to sort rosettes from solitary cells in a mixed culture. Through this flow cytometry-based method, I found that I was able to enrich for rosettes at a significant rate (Fig. A2.2F). Thus, flow cytometry-mediated sorting appears to be the most effective strategy, of those I tried, for selecting rosettes from single cells.

<u>A conditional screen to identify a RIF-receptor</u>

To screen for conditional mutants that respond to cues from one rosette-inducing bacterial species but not another, I first treated SrEpac with 50 mM ENU and isolated a library of clones by limiting dilution. I then replica plated those clones into media containing either *A. machipongonensis* OMVs, *A. muciniphila* OMVs, or *Demequina spp.* conditioned media (Fig. A2.3A). These three species represent diverse bacterial phyla, both Gram-negative and Gram-positive, and all three induce rosette development in *S. rosetta* (88, 94). Importantly, *A. muciniphila* and *Demequina spp.* are not known to produce sulfonolipids, which, in bacteria, thus far have only been described in Bacteroidetes (e.g. (88, 118–120)). Therefore I hypothesized that mutants that formed rosettes in the presence of only a subset of rosette-inducing bacteria would indicate a mutation in a gene required for transducing different rosette-inducing cues.

I screened a total of 10,729 ENU-mutagenized clones, each exposed to *A. machipongonensis*, *A. muciniphila* or *Demequina spp*. From this screen I isolated a single mutant, which did not form rosettes in the presence of any of the rosette-inducing bacteria, and thus did not meet my definition of a conditional mutant. This rosette-defect mutant was categorized as Class C (121), as it formed large clumps in the presence or absence of inducing bacterial cues, and did not ever form rosettes (Fig. A2.3B). My mutant recovery rate was 0.0009%, which was lower than the recovery rates of previous rosette defect screens (0.059% (106) and 0.032% (121)), suggesting that in fact the mutagenesis rate had not improved (Table A2.1).

A constitutive mutant selection to identify a RIF-receptor

In addition to the conditional mutant screen, I performed a screen to isolate a constitutive rosette formation mutant (Fig. A2.4A). First, I split a culture of SrEpac into two conditions: one unmutagenized (to screen for spontaneous mutants), and one treated with 50 mM ENU. Both cultures were passaged for 3 days, then treated with a 1:20,000 dilution of *A. machipongonensis* OMVs for 24 hours, which induced only 1-20% of cells to form rosettes (Fig. A2.4B, arrow marked (1)). I then used flow cytometry to select for the small population of rosettes, which should contain both wild type rosettes, as well as any sensitized or constitutive mutants.

In parallel with the constitutive mutant screen, I performed a control experiment to verify the effectiveness of enriching for rosettes in a mixed population by flow cytometry. I mixed cells from wild type SrEpac with the *rtls*^{l1} mutant of *S. rosetta*, which does not form rosettes (106), at a 1:9 ratio. I treated the mixed culture with a 1:1,000 dilution of *A. machipongonensis* OMVs. This dose is sufficient to induce the majority of the wild type cells to undergo rosette development (Fig. A2.4B, arrow marked (2)), but has no effect on the *rtls*^{l1} mutant, which remains solitary. Thus, after sorting for rosettes, only wild type cells should have been selected.

After selecting for rosettes from the unmutagenized culture, ENU-treated culture and SrEpac/*rtls*^{l1} mix, I then passaged the sorted cultures in the absence of any rosette-inducing signal, a condition under which rosettes break apart and the culture returns to a solitary-celled state. I repeated the *A. machipongonensis* OMV treatment, selection by flow cytometry and passaging for 4 rounds (Fig. A2.4A). If flow cytometry-based selection were effective, I would expect the percentage of rosette-forming (wild type) cells in the SrEpac/*rtls*^{l1} mix to increase after each round of selection. Although the final ratio of rosettes to solitary cells in the culture increased from 0.10 before selection to 1.04 after the fourth round of selection, the increase was not consistent, and the ratio of rosettes to solitary cells actually decreased after the second and third rounds of selection (Fig. A2.4C). When I counted the ratio of rosettes to solitary cells in the unmutagenized and ENU-treated cultures, I did not see a significant enrichment for rosettes after 4 rounds of selection, which might have indicated the presence of rosette-sensitized or constitutive-rosette mutants (Fig. A2.4D). Thus, this experimental approach was unsuccessful in isolating constitutive rosette formation mutants.

Discussion

After screening 10,729 mutagenized clones for a conditional rosette formation mutant, and performing 4 rounds of selection for a constitutive rosette formation mutant, I was unable to isolate either type of mutant. I believe that this is due to an underlying low level of mutagenesis. Despite the seemingly promising results from sequencing mutagenized clones, it is likely that the number of mutations called in the clones was artificially high because I did not filter out low-coverage variants, which may have been simply sequencing errors.

I tested a range of doses of the alkylating agents ENU and EMS, and previous screens used EMS or X-ray mutagenesis (106, 121), but rosette defect mutant recovery rates averaged only 0.035%. This raises the question of why mutagenesis is not very effective in *S. rosetta*. One hypothesis is that *S. rosetta* has very efficient DNA repair machinery. One piece of evidence supporting this can be seen after CRISPR-Cas9-mediated mutagenesis, which results in approximately 20% homology directed repair (HDR; D. S. Booth, unpublished data). While HDR occurs after double stranded DNA breaks (DSBs), it is possible that *S. rosetta* also has very efficient machinery for mismatch repair, or induces DSBs as a response to base alkylation or mismatches, ultimately resulting in HDR. Thus, co-treatment with inhibitors of the DNA damage response may improve mutagenesis (Table A2.2).

Optimizing mutagenesis will allow us to perform efficient forward genetic screens in *S. rosetta* in the future. In addition to testing a range of doses of ENU and EMS, I tested ENU treatment with several different co-treatments in an attempt to improve mutagenesis, but was unsuccessful (Table A2.2). I have also outlined various other co-treatments or mutagenesis methods that may prove useful for future researchers attempting to improve upon current mutagenesis rates (Table A2.2).

Materials and Methods

Choanoflagellate culturing conditions

Artificial seawater (ASW) was prepared by diluting 32.9 g Tropic Marin sea salts in 1L water for a salinity of 32-37 parts per thousand (107). Sea Water Complete media (SWC) was prepared by diluting 5 g/L peptone, 3 g/L yeast extract, and 3 mL/L glycerol in ASW (107). SrEpac (*Salpingoeca rosetta* co-cultured with the prey bacterium *Echinicola pacifica*, ATCC PRA-390; (107)) was cultured in 5% Sea Water Complete media (5% SWC vol/vol in ASW) at 22ºC. Cultures were passaged daily, 1 mL into 9 mL fresh media in 25cm^2 cell culture flasks (Corning).

Chemical mutagenesis

SrEpac cultures were washed 2X in ASW to reduce *E. pacifica* bacteria, and resuspended at 10^7 cells/mL in ASW. Cultures were treated with 0.5-50 mM ENU (*N*-ethyl-*N*-nitrosourea, Sigma), 0.05-5% (vol/vol) EMS (ethyl methanesulfonate, Sigma), or equivalent volumes of DMSO (dimethyl sulfoxide, Sigma) as a carrier control, and incubated on a nutating rocker for 1 hour. The cultures were then pelleted and washed 2X with 5% (wt/vol) sodium thiosulfate (Sigma) in ASW to inactivate the alkylating agents. Cells were resuspended at $5x10^4$ cells/mL in 5% SWC and *E. pacifica* bacteria was added at a 1:1,000 dilution from a log-phase liquid culture. Cultures were passaged for 4 days prior to clonal isolation or rosette induction.

Clonal isolation

Mutagenized cultures were diluted to 1 cell/mL and plated at 100 µL per well in a 96-well plate (Corning). After 5-6 days of growth, clones were collected and the clonal isolation procedure was repeated to ensure that each isolate was truly clonal.

Whole genome resequencing

9 mutagenized clones and the parent SrEpac culture were each expanded into 100 mL 5% SWC, then treated for 24 hours with 20 µg/mL rifampicin (Thermo Fisher) to reduce *E. pacifica* bacteria. *S. rosetta* cells were pelleted and DNA was extracted using the DNeasy kit (Qiagen). Multiplexed, 150 bp paired-end libraries were prepared and sequenced on an Illumina HiSeq 2500 (Vincent J. Coates Genomics Sequencing Laboratory at UC Berkeley, supported by NIH S10 OD018174 Instrumentation Grant). The data were processed and analyzed as in (106). Briefly, raw reads were trimmed with TrimmomaticPE (132) to remove low quality base calls. Trimmed reads were mapped to the *S. rosetta* reference genome (122) using Burrows-Wheeler Aligner (133), and I removed PCR duplicates with Picard (http://broadinstitute.github.io/picard/). I realigned reads surrounding INDEL calls using GATK (134) and called variants using SAMtools and bcftools (135).

Measuring bacterial colony-forming units (CFUs)

To approximate the ratio of choanoflagellate to bacterial cells (Fig. A2.1B), I performed serial 1:10 dilutions, in triplicate, from rifampicin-treated cultures. I

plated 5 µL from each dilution on 100% SWC agar plates, incubated at room temperature for 2-3 days, and counted the number of colonies that formed.

Preparation of bacterial conditioned media and isolation of OMVs

A. machipongongensis (ATCC BAA-2233, (111)) and *Demequina spp.* (94) were grown in 500 mL 100% SWC, shaking at 30ºC for 48 hours. *A. muciniphila* (ATCC BAA-835, (126)) was grown in 500 mL Brain Heart Infusion broth (37 g/L, Sigma) under anaerobic conditions for 7 days. The bacteria were pelleted and the supernatant was filtered through a 0.2 µm filter to produce conditioned media. *A. machipongongensis* and *A. muciniphila* OMVs were prepared by centrifuging conditioned media at 36,000 x g for 3 hours at 4ºC (Type 45 Ti rotor, Beckman Coulter). OMV-containing pellets were resuspended in 2 mL ASW.

Rosette induction

To test different methods for sorting rosettes from solitary cells (Fig. A2.2), untreated SrEpac cultures were mixed with SrEpac cultures that had been treated with a 1:1,000 dilution of *A. machipongonensis* OMVs for 24 hours. For the constitutive mutant screen (Fig. A2.3A), clones were treated with a 1:5,000 dilution of *A. machipongonensis* OMVs, a 1:1,000 dilution of *A. muciniphila* OMVs, or a 1:5 dilution of *Demequina spp.* conditioned media. To determine whether multiple rounds of flow cytometry-based sorting was effective (Fig. A2.4C), SrEpac was mixed with the *rtls*^{l1} mutant at a 1:9 ratio, and the mixed culture was treated with a 1:1,000 dilution of *A. machipongonensis* OMVs for 24 hours before sorting. For the constitutive mutant screen (Fig. A2.4D), cultures were treated with a 1:20,000 dilution of *A. machipongonensis* OMVs for 24 hours.

Rosette sorting

Density gradient centrifugation (Fig. A2.2C): 100 µL mixed rosette and solitary cell cultures were layered on top of a 1 mL 0-80% gradient Percoll in ASW, then centrifuged at 1000xg for 20 minutes (fixed angle rotor, Eppendorf). Samples were collected in 100 µL increments.

Flagellar inhibition (Fig. A2.2D): 10 mL mixed rosette and solitary cell cultures were treated with the dynein inhibitor Ciliobrevin A (Sigma) at a final concentration of 10 µM for 6 hours, to inhibit flagellar motion. Cells were allowed to settle passively during this time, after which samples were collected in 1 mL increments.

Flow cytometry (Fig. A2.2F, Fig. A2.4C-D): Mixed populations of rosettes and solitary cells were sorted based on forward and side scatter on a BD Influx cell sorter (UC Berkeley Flow Cytometry Facility).

Quantification: To quantify the ratio of rosettes to solitary cells, cultures were fixed with 1% formaldehyde, vortexed, mounted on a Bright-Line hemacytometer (Hausser Scientific), and counted on a Leica DMI6000B inverted compound microscope. Rosettes were defined as groups of four or more cells, and were distinguished from swarms based on their resistance to mechanical shear and their stereotypical orientation with their basal poles pointed inwards and their flagella out (104, 106).

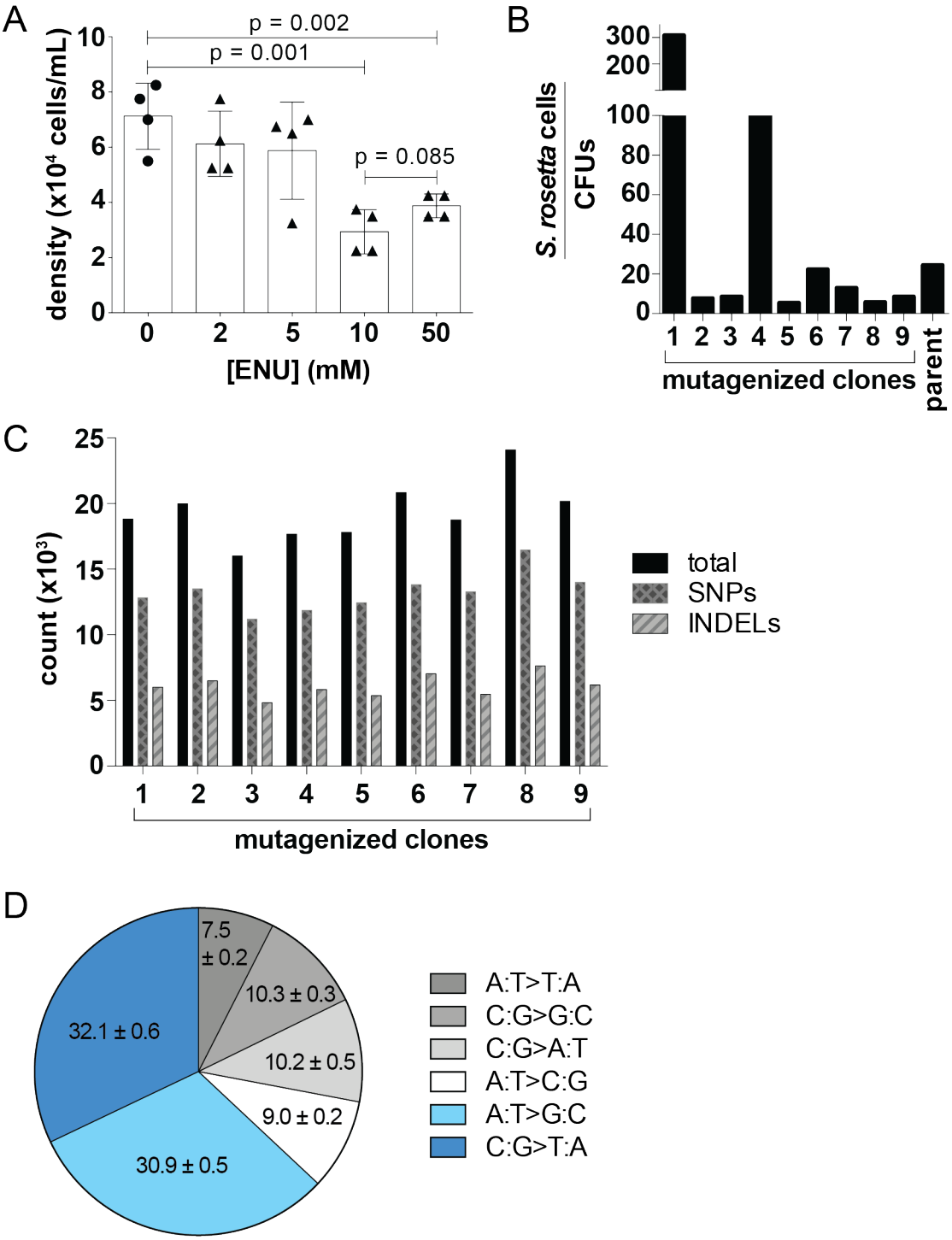

Figure A2.1: Efficiency of ENU mutagenesis
(A) Cell density decreases 24 hours after treatment with 2-50 mM ENU (unpaired *t* test). (B) Treatment of each mutagenized clone and the parent culture with 20 µg/mL rifampicin results in 5.2–308 choanoflagellate cells per bacterial colony forming unit (CFU). (C) Shown are the total number of variants called for each clone

(black bars), number of variants consisting of single nucleotide polymorphisms (SNPs, diamond bars), and number of variants consisting of insertions or deletions (INDELs, striped bars). (D) Shown are the percentages of each transition or transversion out of total SNPs, averaged across all 9 clones (mean ± S.D.).

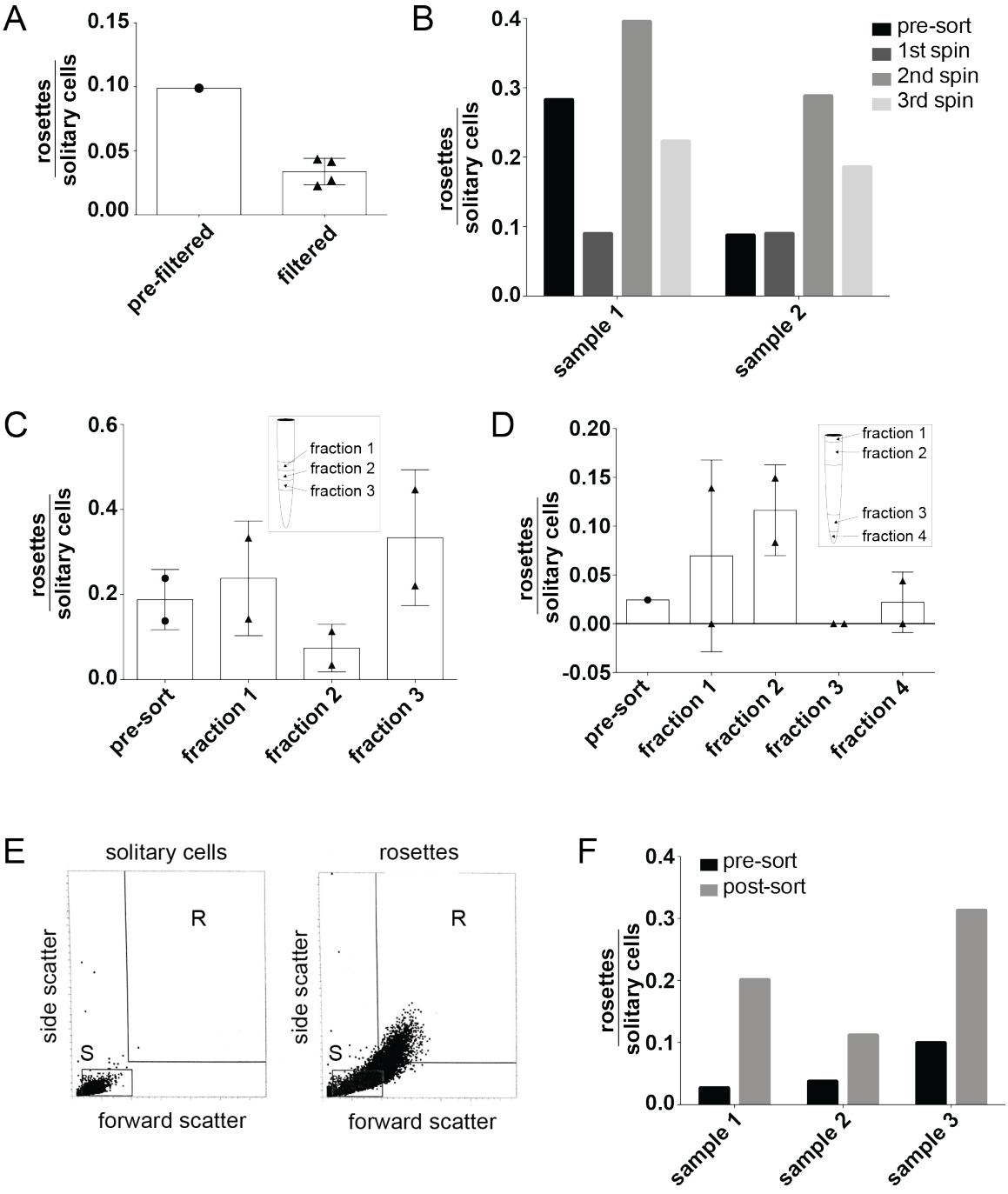

Figure A2.2: Size-based methods for sorting rosettes from a mixed population
(A) Filtration of a mixture of rosettes and solitary cells through an 8 μm membrane does not increase the ratio of rosettes to solitary cells. (B) Centrifugation of a mixture of rosettes and solitary cells at 100xg for 5 minutes does not consistently increase the ratio of rosettes to solitary cells. (C) Density gradient centrifugation of a mixture of rosettes and solitary cells over a 0-80% Percoll column does not effectively separate rosettes from solitary cells. Shown are the ratios of rosettes to

solitary cells for three fractions of different densities (inset). (D) Inhibition of flagellar motion in a mixture of rosettes and solitary cells by treatment with 10 μM Ciliobrevin A, followed by passive settlement for 6 hours, does not effectively separate rosettes from solitary cells. Shown are the ratios of rosettes to solitary cells for four fractions taken after settlement (inset). (E) Flow cytometry plots of side scatter vs forward scatter for a solitary-celled SrEpac culture (left) and a rosette-induced SrEpac culture (treated with a 1:1,000 dilution of *A. machipongonensis* OMVs for 24 hours, right). Gate S was set to include most solitary cells, and gate R was set to include only rosettes. In subsequent experiments, only cells in gate R were collected. (F) Flow cytometry-based sorting of a mixture of rosettes and solitary cells increases the ratio of rosettes to solitary cells in three separate experiments.

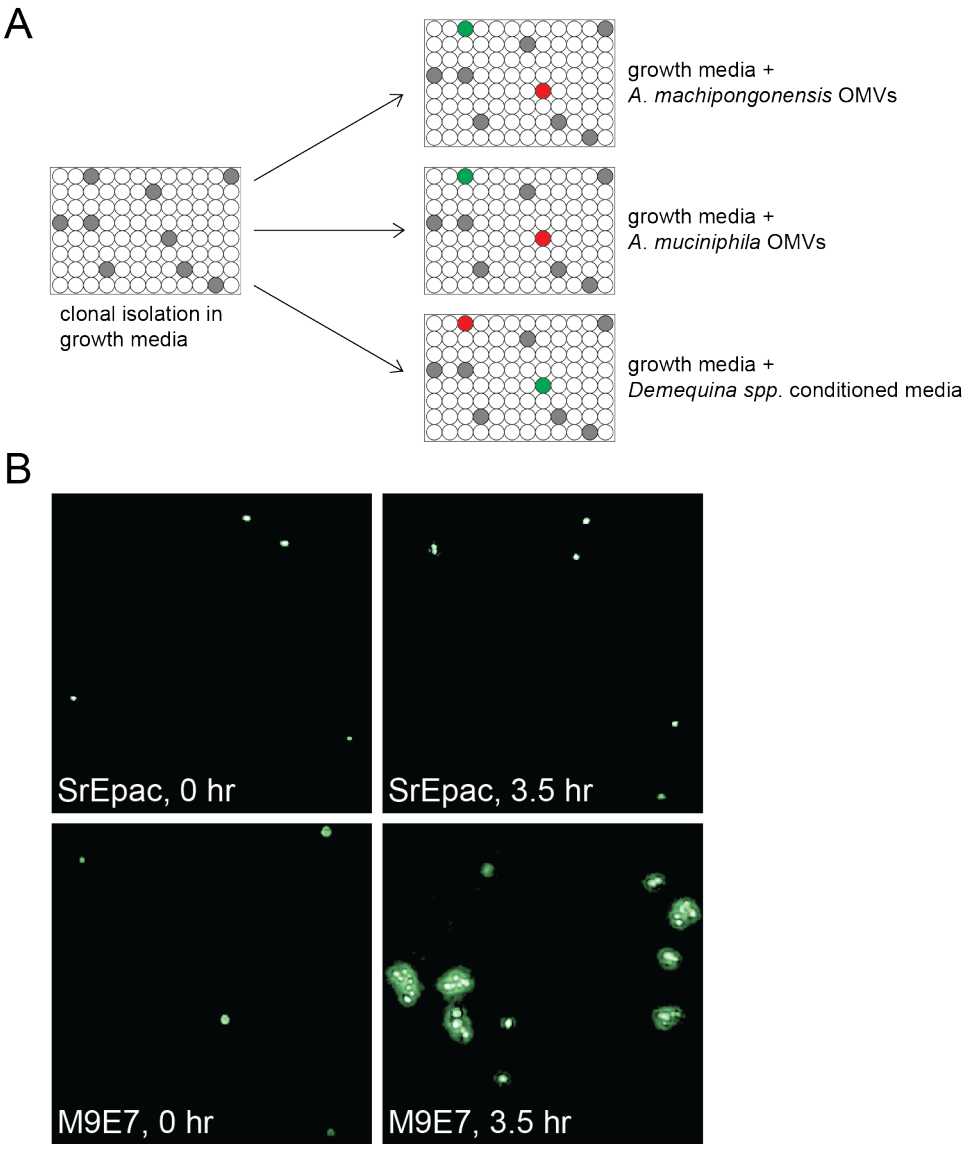

Figure A2.3: Screen for a conditional rosette formation mutant
(A) Schematic of conditional mutant screen. Clones (grey wells) were isolated in growth media, then replica plated into media containing a 1:5,000 dilution of *A. machipongonensis* OMVs, a 1:1,000 dilution of *A. muciniphila* OMVs, or a 1:5 dilution of *Demequina spp.* conditioned media. Plates were screened for mutants that formed rosettes in the presence of one or more inducing bacteria (green wells) but not the other(s) (red wells). (B) Mutant M9E7, isolated as a byproduct of the conditional screen, did not form rosettes but formed clumps of cells within 3.5 hours of vortexing, placing it in rosette defect mutant Class C (121).

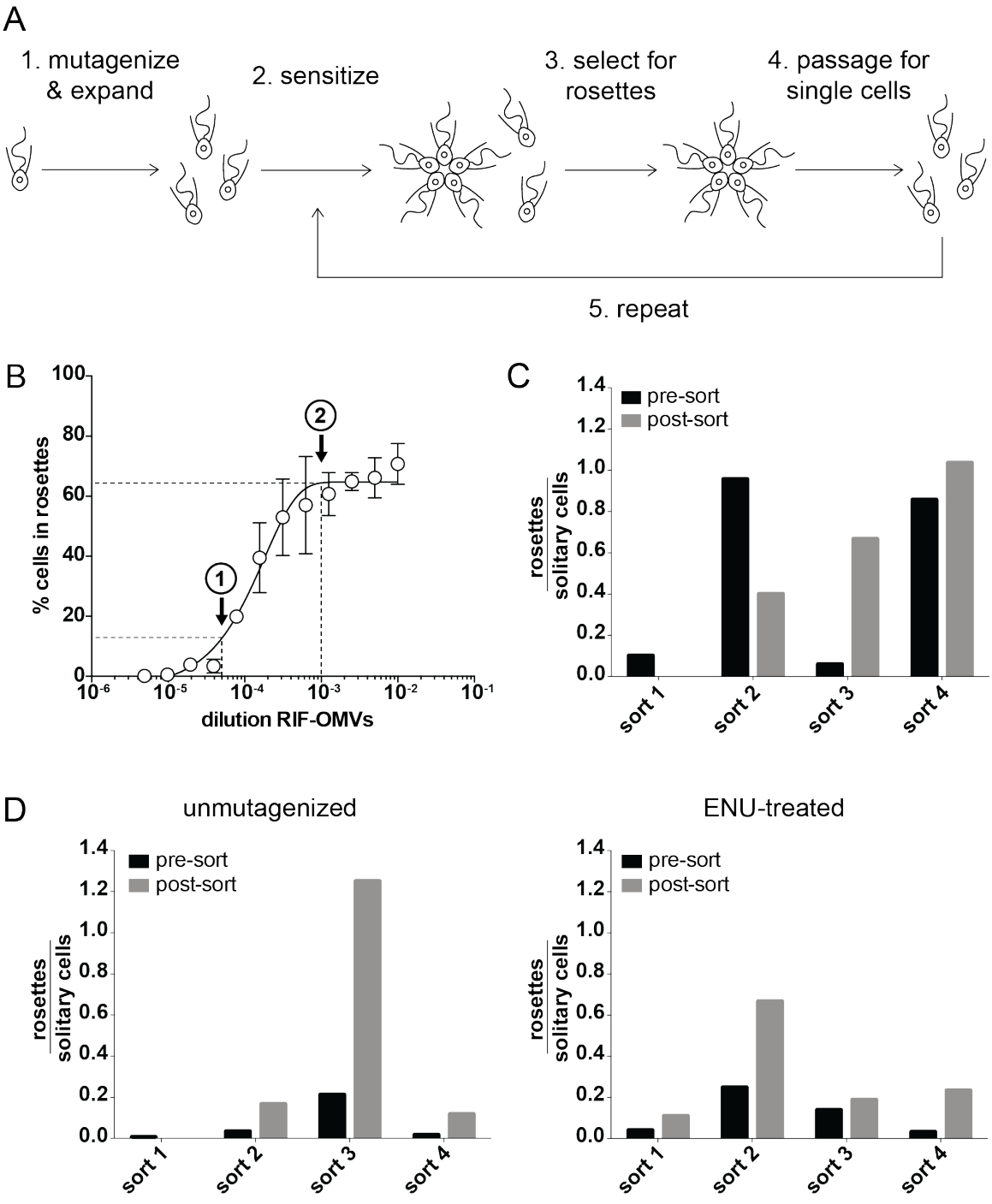

Figure A2.4: Screen for a constitutive rosette formation mutant
(A) Schematic of constitutive mutant screen. A culture of SrEpac was treated with 50 mM ENU (or DMSO for the unmutagenized condition) and passaged for 3 days to expand (1), then treated with a 1:20,000 dilution of *A. machipongonensis* OMVs for 24 hours to sensitize the culture for sorting (2). Rosettes were selected by flow cytometry (3). The sorted cultures were then passaged for several days in the

absence of rosette-inducing signals to allow the cultures to return to a solitary-celled state (4). Steps 2-4 were repeated a total of four times before ending the experiment (5). (B) Serial dilution of *A. machipongonensis* OMVs can be used to drive different percentages of cells in culture into rosettes. A dilution of 1:20,000 was used to sensitize SrEpac cultures for sorting (arrow marked (**1**)), while a dilution of 1:1,000 was used to drive the majority of wild type cells in the SrEpac/*rtls*^{l1} mix into rosettes (arrow marked (**2**)). (C) Flow cytometry-based sorting inconsistently enriches for rosettes from a mixed population. A starting population of 10% SrEpac cells + 90% *rtls*^{l1} cells was treated with a 1:1,000 dilution of *A. machipongonensis* OMVs, then sorted by flow cytometry (sort 1). The sorted cells were passaged, treated with a 1:1,000 dilution of *A. machipongonensis* OMVs, and sorted again (sort 2). This process was repeated a total of 4 times. (D) After 4 rounds of treatment with a 1:20,000 dilution of *A. machipongonensis* OMVs and sorting by flow cytometry, there was not a significant enrichment for rosette-forming cells in unmutagenized (left) or ENU-treated (right) cultures.

Table A2.1: Mutant recovery rates

	# of clones screened	# of mutants recovered	mutant recovery rate
this screen	10,729	1	0.0009%
Levin et al. (106)	15,344	9	0.059%
Wetzel et al. (121)	21,925	7	0.032%

Table A2.2: Methods of improving mutagenesis

Method	Attempted?	Results	Reference
Pretreatment with priming buffer (remove extracellular material coating the cell)	Yes (this study)	No change in cell death	(128)
Pretreatment with aphidicolin (sync cell cycle)	Yes (this study)	No change in cell death	(105, 136)
Pretreatment with other cell cycle inhibitors	No	N/A	(137)
Vary amount of prey bacteria	Yes (this study)	No change in cell death	(138)
Vary media conditions and/or species of prey bacteria	Yes (Levin & King 2013)	Produced "Isolate B" with unique polymorphisms compared to parental strain	(107)
Vary length of incubation in mutagen	No	N/A	(138–140)
Vary life history stage or ploidy	No	N/A	(104, 107)
Induce recombination during mutagenesis	No	N/A	(87, 107, 141)
Disrupt DNA damage repair pathways	No	N/A	(142, 143)
X-ray mutagenesis	Yes (Levin et al. 2014)	40% reduction in cell number, produced several rosette defect mutants	(106)
UV mutagenesis	Yes (Rachel Wang and others, King lab)	No mutants isolated	(144)
CRISPR mutagenesis	In development (David Booth, King lab)	N/A	(145)
Transposon mutagenesis	In development (Monika Sigg, King lab)	N/A	(146)

References

1. Webster NS, Smith LD, Heyward AJ, Watts JEM, Webb RI, Blackall LL, Negri AP. 2004. Metamorphosis of a scleractinian coral in response to microbial biofilms. Appl Environ Microbiol 70:1213–1221.

2. Hadfield MG. 2011. Biofilms and Marine Invertebrate Larvae: What Bacteria Produce That Larvae Use to Choose Settlement Sites. Ann Rev Mar Sci 3:453–470.

3. Shikuma NJ, Pilhofer M, Weiss GL, Hadfield MG, Jensen GJ, Newman DK. 2014. Marine Tubeworm Metamorphosis Induced by Arrays of Bacterial Phage Tail-Like Structures. Science 343:529–533.

4. Woznica A, King N. 2018. Lessons from simple marine models on the bacterial regulation of eukaryotic development. Curr Opin Microbiol 43:108–116.

5. Bates JM, Mittge E, Kuhlman J, Baden KN, Cheesman SE, Guillemin K. 2006. Distinct signals from the microbiota promote different aspects of zebrafish gut differentiation. Dev Biol 297:374–386.

6. Becker S, Oelschlaeger TA, Wullaert A, Pasparakis M, Wehkamp J, Stange EF, Gersemann M. 2013. Bacteria Regulate Intestinal Epithelial Cell Differentiation Factors Both *In Vitro* and *In Vivo*. PLoS One 8:e55620.

7. Bry L, Falk PG, Midtvedt T, Gordon JI. 1996. A model of host-microbial interactions in an open mammalian ecosystem. Science 273:1380–1383.

8. Cheesman SE, Neal JT, Mittge E, Seredick BM, Guillemin K. 2011. Epithelial cell proliferation in the developing zebrafish intestine is regulated by the Wnt pathway and microbial signaling via Myd88. Proc Natl Acad Sci 108:4570–4577.

9. Bouskra D, Brézillon C, Bérard M, Werts C, Varona R, Boneca IG, Eberl G. 2008. Lymphoid tissue genesis induced by commensals through NOD1 regulates intestinal homeostasis. Nature 456:507–510.

10. Mazmanian SK, Liu CH, Tzianabos AO, Kasper DL. 2005. An immunomodulatory molecule of symbiotic bacteria directs maturation of the host immune system. Cell 122:107–118.

11. Chung H, Pamp SJ, Hill JA, Surana NK, Edelman SM, Troy EB, Reading NC, Villablanca EJ, Wang S, Mora JR, Umesaki Y, Mathis D, Benoist C, Relman DA, Kasper DL. 2012. Gut immune maturation depends on colonization with a host-specific microbiota. Cell 149:1578–1593.

12. Olszak T, An D, Zeissig S, Vera MP, Richter J, Franke A, Glickman JN, Siebert R,

Baron RM, Kasper DL, Blumberg RS. 2012. Microbial Exposure During Early Life Has Persistent Effects on Natural Killer T Cell Function. Science 336:489–493.

13. Heijtz RD, Wang S, Anuar F, Qian Y, Bjorkholm B, Samuelsson A, Hibberd ML, Forssberg H, Pettersson S. 2011. Normal gut microbiota modulates brain development and behavior. Proc Natl Acad Sci 108:3047–3052.

14. Sharon G, Sampson TR, Geschwind DH, Mazmanian SK. 2016. The Central Nervous System and the Gut Microbiome. Cell 167:915–932.

15. Round JL, Mazmanian SK. 2009. The gut microbiota shapes intestinal immune responses during health and disease. Nat Rev Immunol 9:313–323.

16. Lipkin WI. 2008. Pathogen Discovery. PLoS Pathog 4:e1000002.

17. Carmody RN, Gerber GK, Luevano JM, Gatti DM, Somes L, Svenson KL, Turnbaugh PJ. 2015. Diet dominates host genotype in shaping the murine gut microbiota. Cell Host Microbe 17:72–84.

18. Wu GD, Chen J, Hoffmann C, Bittinger K, Chen Y-Y, Keilbaugh SA, Bewtra M, Knights D, Walters WA, Knight R, Sinha R, Gilroy E, Gupta K, Baldassano R, Nessel L, Li H, Bushman FD, Lewis JD. 2011. Linking Long-Term Dietary Patterns with Gut Microbial Enterotypes. Science 334:105–108.

19. Turnbaugh PJ, Ridaura VK, Faith JJ, Rey FE, Knight R, Gordon JI. 2009. The Effect of Diet on the Human Gut Microbiome: A Metagenomic Analysis in Humanized Gnotobiotic Mice. Sci Transl Med 1:6ra14.

20. Wexler HM. 2007. *Bacteroides*: The good, the bad, and the nitty-gritty. Clin Microbiol Rev 20:593–621.

21. Townsend GE, Han W, Schwalm ND, Raghavan V, Barry NA, Goodman AL, Groisman EA. 2019. Dietary sugar silences a colonization factor in a mammalian gut symbiont. Proc Natl Acad Sci 116:233–238.

22. Sonnenburg JL, Xu J, Leip DD, Chen C-H, Westover BP, Weatherford J, Buhler JD, Gordon JI. 2005. Glycan Foraging in Vivo by an Intestine-Adapted Bacterial Symbiont. Science 307:1955–1959.

23. Porter NT, Canales P, Peterson DA, Martens EC. 2017. A Subset of Polysaccharide Capsules in the Human Symbiont *Bacteroides thetaiotaomicron* Promote Increased Competitive Fitness in the Mouse Gut. Cell Host Microbe 22:494–506.

24. Bjursell MK, Martens EC, Gordon JI. 2006. Functional genomic and metabolic studies of the adaptations of a prominent adult human gut symbiont,

Bacteroides thetaiotaomicron, to the suckling period. J Biol Chem 281:36269–36279.

25. Sun X, Stefanetti G, Berti F, Kasper DL. 2019. Polysaccharide structure dictates mechanism of adaptive immune response to glycoconjugate vaccines. Proc Natl Acad Sci 116:193–198.

26. Wegorzewska MM, P Glowacki RW, Hsieh SA, Donermeyer DL, Hickey CA, Horvath SC, Martens EC, Stappenbeck TS, Allen PM. 2019. Diet modulates colonic T cell responses by regulating the expression of a *Bacteroides thetaiotaomicron* antigen. Sci Immunol 4:eaau9079.

27. Ruby EG, McFall-Ngai MJ. 1992. A squid that glows in the night: Development of an animal-bacterial mutualism. J Bacteriol 174:4865–4870.

28. Jones BW, Nishiguchi MK. 2004. Counterillumination in the Hawaiian bobtail squid, *Euprymna scolopes* Berry (Mollusca: Cephalopoda). Mar Biol 144:1151–1155.

29. Norsworthy AN, Visick KL. 2013. Gimme shelter: how *Vibrio fischeri* successfully navigates an animal's multiple environments. Front Microbiol 4:356.

30. Davidson SK, Koropatnick TA, Kossmehl R, Sycuro L, McFall-Ngai MJ. 2004. NO means "yes" in the squid-vibrio symbiosis: Nitric oxide (NO) during the initial stages of a beneficial association. Cell Microbiol 6:1139–1151.

31. Wang Y, Dunn AK, Wilneff J, McFall-Ngai MJ, Spiro S, Ruby EG. 2010. *Vibrio fischeri* flavohaemoglobin protects against nitric oxide during initiation of the squid-*Vibrio* symbiosis. Mol Microbiol 78:903–915.

32. Ruby EG, McFall-Ngai MJ. 1999. Oxygen-utilizing reactions and symbiotic colonization of the squid light organ by *Vibrio fischeri*. Trends Microbiol 7:414–420.

33. Altura MA, Stabb E, Goldman W, Apicella M, Mcfall-Ngai MJ. 2011. Attenuation of host NO production by MAMPs potentiates development of the host in the squid-vibrio symbiosis. Cell Microbiol 13:527–537.

34. Weis VM, Small AL, Mcfall-Ngai MJ. 1996. A peroxidase related to the mammalian antimicrobial protein myeloperoxidase in the *Euprymna*-*Vibrio* mutualism. Proc Natl Acad Sci 93:13683–13688.

35. DeLoney-Marino CR, Wolfe AJ, Visick KL. 2003. Chemoattraction of *Vibrio fischeri* to Serine, Nucleosides, and *N*-Acetylneuraminic Acid, a Component of Squid Light-Organ Mucus. Appl Environ Microbiol 69:7527–7530.

36. Mandel MJ, Schaefer AL, Brennan CA, Heath-Heckman EAC, DeLoney-Marino CR, McFall-Ngai MJ, Ruby EG. 2012. Squid-derived chitin oligosaccharides are a chemotactic signal during colonization by *Vibrio fischeri*. Appl Environ Microbiol 78:4620–4626.

37. Boettcher KJ, Ruby EG. 1990. Depressed Light Emission by Symbiotic *Vibrio fischeri* of the Sepiolid Squid *Euprymna scolopes*. J Bacteriol 172:3701–3706.

38. Lyell NL, Dunn AK, Bose JL, Stabb E V. 2010. Bright Mutants of *Vibrio fischeri* ES114 Reveal Conditions and Regulators That Control Bioluminescence and Expression of the *lux* Operon. J Bacteriol 192:5103–5114.

39. Septer AN, Lyell NL, Stabb E V. 2013. The Iron-Dependent Regulator Fur Controls Pheromone Signaling Systems and Luminescence in the Squid Symbiont *Vibrio fischeri* ES114. Appl Environ Microbiol 79:1826–1834.

40. Bose JL, Kim U, Bartkowski W, Gunsalus RP, Overley AM, Lyell NL, Visick KL, Stabb E V. 2007. Bioluminescence in *Vibrio fischeri* is controlled by the redox-responsive regulator ArcA. Mol Microbiol 65:538–553.

41. Van Opijnen T, Breeuwer JAJ. 1999. High temperatures eliminate *Wolbachia*, a cytoplasmic incompatibility inducing endosymbiont, from the two-spotted spider mite. Exp Appl Acarol 23:871–881.

42. Russell JA, Moran NA. 2006. Costs and benefits of symbiont infection in aphids: variation among symbionts and across temperatures. Proc R Soc B Biol Sci 273:603–610.

43. Garcia-Gutierrez E, Mayer MJ, Cotter PD, Narbad A. 2019. Gut microbiota as a source of novel antimicrobials. Gut Microbes 10:1–21.

44. Sassone-Corsi M, Nuccio SP, Liu H, Hernandez D, Vu CT, Takahashi AA, Edwards RA, Raffatellu M. 2016. Microcins mediate competition among Enterobacteriaceae in the inflamed gut. Nature 540:280–283.

45. den Besten G, van Eunen K, Groen AK, Venema K, Reijngoud D-J, Bakker BM. 2013. The role of short-chain fatty acids in the interplay between diet, gut microbiota, and host energy metabolism. J Lipid Res 54:2325–2340.

46. Jacobson A, Lam L, Rajendram M, Tamburini F, Honeycutt J, Pham T, Van Treuren W, Pruss K, Stabler SR, Lugo K, Bouley DM, Vilches-Moure JG, Smith M, Sonnenburg JL, Bhatt AS, Huang KC, Monack D. 2018. A Gut Commensal-Produced Metabolite Mediates Colonization Resistance to *Salmonella* Infection. Cell Host Microbe 24:296–307.

47. Gantois I, Ducatelle R, Pasmans F, Haesebrouck F, Hautefort I, Thompson A, Hinton JC, Van Immerseel F. 2006. Butyrate Specifically Down-Regulates

Salmonella Pathogenicity Island 1 Gene Expression. Appl Environ Microbiol 72:946–949.

48. Hung CC, Garner CD, Slauch JM, Dwyer ZW, Lawhon SD, Frye JG, Mcclelland M, Ahmer BMM, Altier C. 2013. The intestinal fatty acid propionate inhibits *Salmonella* invasion through the post-translational control of HilD. Mol Microbiol 87:1045–1060.

49. Maier L, Vyas R, Cordova CD, Lindsay H, Schmidt TSB, Brugiroux S, Periaswamy B, Bauer R, Sturm A, Schreiber F, von Mering C, Robinson MD, Stecher B, Hardt W-D. 2013. Microbiota-Derived Hydrogen Fuels *Salmonella* Typhimurium Invasion of the Gut Ecosystem. Cell Host Microbe 14:641–651.

50. Ng KM, Ferreyra JA, Higginbottom SK, Lynch JB, Kashyap PC, Gopinath S, Naidu N, Choudhury B, Weimer BC, Monack DM, Sonnenburg JL. 2013. Microbiota-liberated host sugars facilitate post-antibiotic expansion of enteric pathogens. Nature 502:96–99.

51. Crouch ML V, Castor M, Karlinsey JE, Kalhorn T, Fang FC. 2008. Biosynthesis and IroC-dependent export of the siderophore salmochelin are essential for virulence of *Salmonella enterica* serovar Typhimurium. Mol Microbiol 67:971–983.

52. Sassone-Corsi M, Chairatana P, Zheng T, Perez-Lopez A, Edwards RA, George MD, Nolan EM, Raffatellu M. 2016. Siderophore-based immunization strategy to inhibit growth of enteric pathogens. Proc Natl Acad Sci 113:13462–13467.

53. Deriu E, Liu JZ, Pezeshki M, Edwards RA, Ochoa RJ, Contreras H, Libby SJ, Fang FC, Raffatellu M. 2013. Probiotic Bacteria Reduce *Salmonella* Typhimurium Intestinal Colonization by Competing for Iron. Cell Host Microbe 14:26–37.

54. Ryan RP, Fouhy Y, Garcia BF, Watt SA, Niehaus K, Yang L, Tolker-Nielsen T, Dow JM. 2008. Interspecies signalling via the *Stenotrophomonas maltophilia* diffusible signal factor influences biofilm formation and polymyxin tolerance in *Pseudomonas aeruginosa*. Mol Microbiol 68:75–86.

55. Twomey KB, O'Connell OJ, McCarthy Y, Dow JM, O'Toole GA, Plant BJ, Ryan RP. 2012. Bacterial cis-2-unsaturated fatty acids found in the cystic fibrosis airway modulate virulence and persistence of *Pseudomonas aeruginosa*. ISME J 6:939–950.

56. Orazi G, Ruoff KL, O'Toole GA. 2019. *Pseudomonas aeruginosa* increases the sensitivity of biofilm-grown *Staphylococcus aureus* to membrane-targeting antiseptics and antibiotics. bioRxiv http://dx.doi.org/10.1101/668780.

57. Orazi G, O'Toole GA. 2017. *Pseudomonas aeruginosa* Alters *Staphylococcus aureus* Sensitivity to Vancomycin in a Biofilm Model of Cystic Fibrosis

Infection. MBio 8:1420–1438.

58. Ramsey MM, Freire MO, Gabrilska RA, Rumbaugh KP, Lemon KP. 2016. *Staphylococcus aureus* Shifts toward Commensalism in Response to *Corynebacterium* Species. Front Microbiol 7:1230.

59. Hurlbut GD, Kankel MW, Artavanis-tsakonas S. 2009. Nodal points and complexity of Notch-Ras. Proc Natl Acad Sci 106:2218–23.

60. McNeill H, Woodgett JR. 2010. When pathways collide: Collaboration and connivance among signalling proteins in development. Nat Rev Mol Cell Biol 11:404–413.

61. Tanoue T, Morita S, Plichta DR, Skelly AN, Suda W, Sugiura Y, Narushima S, Vlamakis H, Motoo I, Sugita K, Shiota A, Takeshita K, Yasuma-Mitobe K, Riethmacher D, Kaisho T, Norman JM, Mucida D, Suematsu M, Yaguchi T, Bucci V, Inoue T, Kawakami Y, Olle B, Roberts B, Hattori M, Xavier RJ, Atarashi K, Honda K. 2019. A defined commensal consortium elicits CD8 T cells and anti-cancer immunity. Nature 565:600–605.

62. Atarashi K, Tanoue T, Oshima K, Suda W, Nagano Y, Nishikawa H, Fukuda S, Saito T, Narushima S, Hase K, Kim S, Fritz J V, Wilmes P, Ueha S, Matsushima K, Ohno H, Olle B, Sakaguchi S, Taniguchi T, Morita H, Hattori M, Honda K. 2013. Treg induction by a rationally selected mixture of Clostridia strains from the human microbiota. Nature 500:232–236.

63. Sibley CD, Duan K, Fischer C, Parkins MD, Storey DG, Rabin HR, Surette MG. 2008. Discerning the complexity of community interactions using a *Drosophila* model of polymicrobial infections. PLoS Pathog 4:e1000184.

64. Napolitani G, Rinaldi A, Bertoni F, Sallusto F, Lanzavecchia A. 2005. Selected Toll-like receptor agonist combinations synergistically trigger a T helper type 1 -polarizing program in dendritic cells. Nat Immunol 6:769–776.

65. Kellogg RA, Tian C, Etzrodt M, Tay S. 2017. Cellular Decision Making by Non-Integrative Processing of TLR Inputs. Cell Rep 19:125–135.

66. Trinchieri G, Sher A. 2007. Cooperation of Toll-like receptor signals in innate immune defence. Nat Rev Immunol 7:179–190.

67. Ratner AJ, Lysenko ES, Paul MN, Weiser JN. 2005. Synergistic proinflammatory responses induced by polymicrobial colonization of epithelial surfaces. Proc Natl Acad Sci 102:3429–3434.

68. Murillo-Rincon AP, Klimovich A, Pemöller E, Taubenheim J, Mortzfeld B, Augustin R, Bosch TCG. 2017. Spontaneous body contractions are modulated by the microbiome of *Hydra*. Sci Rep 7:15937.

69. Fraune S, Anton-Erxleben F, Augustin R, Franzenburg S, Knop M, Schröder K, Willoweit-Ohl D, Bosch TC. 2015. Bacteria–bacteria interactions within the microbiota of the ancestral metazoan *Hydra* contribute to fungal resistance. ISME J 9:1543–1556.

70. Tran C, Hadfield M. 2011. Larvae of *Pocillopora damicornis* (Anthozoa) settle and metamorphose in response to surface-biofilm bacteria. Mar Ecol Prog Ser 433:85–96.

71. Nielsen SJ, Harder T, Steinberg PD. 2015. Sea urchin larvae decipher the epiphytic bacterial community composition when selecting sites for attachment and metamorphosis. FEMS Microbiol Ecol 91.

72. Foster JS, Apicella MA, McFall-Ngai MJ. 2000. *Vibrio fischeri* lipopolysaccharide induces developmental apoptosis, but not complete morphogenesis, of the *Euprymna scolopes* symbiotic light organ. Dev Biol 226:242–254.

73. Koropatnick TA, Engle JT, Apicella MA, Stabb E V., Goldman WE, McFall-Ngai MJ. 2004. Microbial factor-mediated development in a host-bacterial mutualism. Science 306:1186–1188.

74. Eckburg PB, Bik EM, Bernstein CN, Purdom E, Dethlefsen L, Sargent M, Gill SR, Nelson KE, Relman DA. 2005. Diversity of the human intestinal microbial flora. Science 308:1635–1638.

75. Lagkouvardos I, Overmann J, Clavel T. 2017. Cultured microbes represent a substantial fraction of the human and mouse gut microbiota. Gut Microbes 8:493–503.

76. Lozupone CA, Stombaugh JI, Gordon JI, Jansson JK, Knight R. 2012. Diversity, stability and resilience of the human gut microbiota. Nature 489:220–230.

77. Donia MS, Fischbach MA. 2015. Small molecules from the human microbiota. Science 349:1254766.

78. Dorrestein PC, Mazmanian SK, Knight R. 2014. Finding the Missing Links among Metabolites, Microbes, and the Host. Immunity 40:824–832.

79. Lang BF, OKelly C, Nerad T, Gray MW, Burger G. 2002. The Closest Unicellular Relatives of Animals. Curr Biol 12:1773–1778.

80. King N, Westbrook MJ, Young SL, Kuo A, Abedin M, Chapman J, Fairclough S, Hellsten U, Isogai Y, Letunic I, Marr M, Pincus D, Putnam N, Rokas A, Wright KJ, Zuzow R, Dirks W, Good M, Goodstein D, Lemons D, Li W, Lyons JB, Morris A, Nichols S, Richter DJ, Salamov A, Sequencing JGI, Bork P, Lim WA, Manning G, Miller WT, McGinnis W, Shapiro H, Tjian R, Grigoriev I V, Rokhsar D. 2008. The genome of the choanoflagellate *Monosiga brevicollis* and the origin of

metazoans. Nature 451:783–788.

81. Ruiz-Trillo I, Roger AJ, Burger G, Gray MW, Lang BF. 2008. A Phylogenomic Investigation into the Origin of Metazoa. Mol Biol Evol 25:664–672.

82. McFall-Ngai M, Hadfield MG, Bosch TCG, Carey H V, Domazet-Lošo T, Douglas AE, Dubilier N, Eberl G, Fukami T, Gilbert SF, Hentschel U, King N, Kjelleberg S, Knoll AH, Kremer N, Mazmanian SK, Metcalf JL, Nealson K, Pierce NE, Rawls JF, Reid A, Ruby EG, Rumpho M, Sanders JG, Tautz D, Wernegreen JJ. 2013. Animals in a bacterial world, a new imperative for the life sciences. Proc Natl Acad Sci 110:3229–3236.

83. Alegado RA, King N. 2014. Bacterial influences on animal origins. Cold Spring Harb Perspect Biol 6:a016162.

84. Richter DJ, King N. 2013. The Genomic and Cellular Foundations of Animal Origins. Annu Rev Genet 47:509–537.

85. Knoll AH. 2011. The Multiple Origins of Complex Multicellularity. Annu Rev Earth Planet Sci 39:217–239.

86. Narbonne GM. 2005. The Ediacara Biota: Neoproterozoic Origin of Animals and Their Ecosystems. Annu Rev Earth Planet Sci 33:421–442.

87. Woznica A, Gerdt JP, Hulett RE, Clardy J, King N. 2017. Mating in the closest living relatives of animals is induced by a bacterial chondroitinase. Cell 170:1–9.

88. Alegado RA, Brown LW, Cao S, Dermenjian RK, Zuzow R, Fairclough SR, Clardy J, King N. 2012. A bacterial sulfonolipid triggers multicellular development in the closest living relatives of animals. eLife 1:e00013.

89. Woznica A, Cantley AM, Beemelmanns C, Freinkman E, Clardy J, King N. 2016. Bacterial lipids activate, synergize, and inhibit a developmental switch in choanoflagellates. Proc Natl Acad Sci 113:7894–7899.

90. Beemelmanns C, Woznica A, Alegado RA, Cantley AM, King N, Clardy J. 2014. Synthesis of the rosette-inducing factor RIF-1 and analogs. J Am Chem Soc 136:10210–10213.

91. Cantley AM, Woznica A, Beemelmanns C, King N, Clardy J. 2016. Isolation and synthesis of a bacterially produced inhibitor of rosette development in choanoflagellates. J Am Chem Soc 138:4326–4329.

92. Casadevall A, Fu M, Guimaraes A, Albuquerque P. 2019. The 'Amoeboid Predator-Fungal Animal Virulence' Hypothesis. J Fungi 5.

93. McFall-Ngai MJ. 2014. The Importance of Microbes in Animal Development: Lessons from the Squid-*Vibrio* Symbiosis. Annu Rev Microbiol 68:177–194.

94. Woznica A. 2017. Bacterial cues regulate multicellular development and mating in the choanoflagellate, *S. rosetta*. PhD thesis. University of California, Berkeley, CA.

95. Derrien M, Belzer C, de Vos WM. 2016. *Akkermansia muciniphila* and its role in regulating host functions. Microb Pathog 106:1–11.

96. Johnson EL, Heaver SL, Walters WA, Ley RE. 2017. Microbiome and metabolic disease: revisiting the bacterial phylum Bacteroidetes. J Mol Med 95:1–8.

97. McFall-Ngai MJ. 2002. Unseen forces: The influence of bacteria on animal development. Dev Biol 242:1–14.

98. Martin R, Nauta AJ, Ben Amor K, Knippels LMJ, Knol J, Garssen J. 2010. Early life: Gut microbiota and immune development in infancy. Benef Microbes 1:367–382.

99. Afkhami ME, Rudgers JA, Stachowicz JJ. 2014. Multiple mutualist effects: conflict and synergy in multispecies mutualisms. Ecology 95:833–844.

100. Mushegian AA, Ebert D. 2016. Rethinking "mutualism" in diverse host-symbiont communities. BioEssays 38:100–108.

101. Dayel MJ, King N. 2014. Prey Capture and Phagocytosis in the Choanoflagellate *Salpingoeca rosetta*. PLoS One 9:e95577.

102. Leadbeater BSC. 2015. The collared flagellate: functional morphology and ultrastructure, p. 18–43. *In* The Choanoflagellates. Cambridge University Press, Cambridge.

103. Tebben J, Tapiolas DM, Motti CA, Abrego D, Negri AP, Blackall LL, Steinberg PD, Harder T. 2011. Induction of Larval Metamorphosis of the Coral *Acropora millepora* by Tetrabromopyrrole Isolated from a *Pseudoalteromonas* Bacterium. PLoS One 6:e19082.

104. Dayel MJ, Alegado RA, Fairclough SR, Levin TC, Nichols SA, McDonald K, King N. 2011. Cell differentiation and morphogenesis in the colony-forming choanoflagellate *Salpingoeca rosetta*. Dev Biol 357:73–82.

105. Fairclough SR, Dayel MJ, King N. 2010. Multicellular development in a choanoflagellate. Curr Biol 20:R875–R876.

106. Levin TC, Greaney AJ, Wetzel L, King N. 2014. The *rosetteless* gene controls development in the choanoflagellate *S. rosetta*. eLife 3:e04070.

107. Levin TC, King N. 2013. Evidence for sex and recombination in the choanoflagellate *Salpingoeca rosetta*. Curr Biol 23:2176–2180.

108. Chandler KB, Leon DR, Kuang J, Meyer RD, Rahimi N, Costello CE. 2019. N-glycosylation regulates ligand-dependent activation and signaling of vascular endothelial growth factor receptor 2 (VEGFR2). J Biol Chem jbc.RA119.008643.

109. Richter DJ, Fozouni P, Eisen MB, King N. 2017. The ancestral animal genetic toolkit revealed by diverse choanoflagellate transcriptomes. bioRxiv http://dx.doi.org/10.1101/211789.

110. Larson BT, Ruiz-Herrero T, Lee S, Kumar S, King N. 2019. Biophysical principles of choanoflagellate self-organization. bioRxiv http://dx.doi.org/10.1101/659698.

111. Alegado RA, Grabenstatter JD, Zuzow R, Morris A, Huang SY, Summons RE, King N. 2013. *Algoriphagus machipongonensis* sp. nov., co-isolated with a colonial choanoflagellate. Int J Syst Evol Microbiol 63:163–168.

112. Matsuo Y, Suzuki M, Kasai H, Shizuri Y, Harayama S. 2003. Isolation and phylogenetic characterization of bacteria capable of inducing differentiation in the green alga *Monostroma oxyspermum*. Environ Microbiol 5:25–35.

113. Grimes DJ, Johnson CN, Dillon KS, Flowers AR, Noriea NF, Berutti T. 2009. What genomic sequence information has revealed about *Vibrio* ecology in the ocean. Microb Ecol 58:447–460.

114. Takemura AF, Chien DM, Polz MF. 2014. Associations and dynamics of Vibrionaceae in the environment, from the genus to the population level. Front Microbiol 5:1–26.

115. van der Heijden MG, Bruin S De, Luckerhoff L, van Logtestijn RS, Schlaeppi K. 2016. A widespread plant-fungal-bacterial symbiosis promotes plant biodiversity, plant nutrition and seedling recruitment. ISME J 10:389–399.

116. Murray JL, Connell JL, Stacy A, Turner KH, Whiteley M. 2014. Mechanisms of synergy in polymicrobial infections. J Microbiol 52:188–199.

117. Kroczek RA, Mages HW, Hutloff A. 2004. Emerging paradigms of T-cell co-stimulation. Curr Opin Immunol 16:321–327.

118. Walker A, Pfitzner B, Harir M, Schaubeck M, Calasan J, Heinzmann SS, Turaev D, Rattei T, Endesfelder D, Castell W zu, Haller D, Schmid M, Hartmann A, Schmitt-Kopplin P. 2017. Sulfonolipids as novel metabolite markers of *Alistipes* and *Odoribacter* affected by high-fat diets. Sci Rep 7:11047.

119. Godchaux W, Leadbetter ER. 1983. Unusual Sulfonolipids Are Characterstic of the *Cytophaga-Flexibacter* Group. J Bacteriol 153:1238–1246.

120. Geiger O, González-Silva N, López-Lara IM, Sohlenkamp C. 2010. Amino acid-containing membrane lipids in bacteria. Prog Lipid Res 49:46–60.

121. Wetzel LA, King N, Levin TC, Hulett RE, Chan D, King GA, Aldayafleh R, Booth DS, Sigg MA, King N. 2018. Predicted glycosyltransferases promote development and prevent spurious cell clumping in the choanoflagellate *S. rosetta*. eLife 7:e41482.

122. Fairclough SR, Chen Z, Kramer E, Zeng Q, Young S, Robertson HM, Begovic E, Richter DJ, Russ C, Westbrook MJ, Manning G, Lang BF, Haas B, Nusbaum C, King N. 2013. Premetazoan genome evolution and the regulation of cell differentiation in the choanoflagellate *Salpingoeca rosetta*. Genome Biol 14:R15.

123. Mouw JK, Ou G, Weaver VM. 2014. Extracellular matrix assembly: a multiscale deconstruction. Nat Rev Mol Cell Biol 15:771–785.

124. Carey DJ. 1997. Syndecans: multifunctional cell-surface co-receptors. Biochem J 327:1–16.

125. Matsuo I, Kimura-Yoshida C. 2013. Extracellular modulation of Fibroblast Growth Factor signaling through heparan sulfate proteoglycans in mammalian development. Curr Opin Genet Dev 23:399–407.

126. Derrien M, Vaughan EE, Plugge CM, Vos WM de. 2004. *Akkermansia muciniphila* gen. nov., sp. nov., a human intestinal mucin-degrading bacterium. Int J Syst Evol Microbiol 54:1469–1476.

127. King N. 2004. The Unicellular Ancestry of Animal Development. Dev Cell 7:313–325.

128. Booth DS, Szmidt-Middleton H, King N. 2018. Transfection of choanoflagellates illuminates their cell biology and the ancestry of animal septins. Mol Biol Cell 29:3026–3038.

129. Koller PC. 1948. The genetical effect of chemical agents on the cell. Proc Intern Congr Genet 8th Congr, Stockholm 45:320–4.

130. Kirkegaard JB, Marron AO, Goldstein RE. 2016. Motility of Colonial Choanoflagellates and the Statistics of Aggregate Random Walkers. Phys Rev Lett 116:38102–38106.

131. Roper M, Dayel MJ, Pepper RE, Koehl MAR. 2013. Cooperatively Generated Stresslet Flows Supply Fresh Fluid to Multicellular Choanoflagellate Colonies.

Phys Rev Lett 110:228104.

132. Bolger AM, Lohse M, Usadel B. 2014. Trimmomatic: A flexible trimmer for Illumina sequence data. Bioinformatics 30:2114–2120.

133. Li H, Durbin R. 2009. Fast and accurate short read alignment with Burrows-Wheeler transform. Bioinformatics 25:1754–1760.

134. Depristo MA, Banks E, Poplin R, Garimella K V., Maguire JR, Hartl C, Philippakis AA, Del Angel G, Rivas MA, Hanna M, McKenna A, Fennell TJ, Kernytsky AM, Sivachenko AY, Cibulskis K, Gabriel SB, Altshuler D, Daly MJ. 2011. A framework for variation discovery and genotyping using next-generation DNA sequencing data. Nat Genet 43:491–501.

135. Li H, Handsaker B, Wysoker A, Fennell T, Ruan J, Homer N, Marth G, Abecasis G, Durbin R. 2009. The Sequence Alignment/Map format and SAMtools. Bioinformatics 25:2078–2079.

136. Goth-Goldstein R, John Burki H. 1980. Ethylnitrosourea-induced mutagenesis in asynchronous and synchronous Chinese hamster ovary cells. Mutat Res 69:127–137.

137. Senese S, Lo YC, Huang D, Zangle TA, Gholkar AA, Robert L, Homet B, Ribas A, Summers MK, Teitell MA, Damoiseaux R, Torres JZ. 2014. Chemical dissection of the cell cycle: Probes for cell biology and anti-cancer drug development. Cell Death Dis 5:e1462.

138. Hince TA, Neale S. 1974. A comparison of the mutagenic action of the methyl and ethyl derivatives of nitrosamides and nitrosamidines on *Escherichia coli*. Mutat Res 24:383–387.

139. De Stasio EA, Dorman S. 2001. Optimization of ENU mutagenesis of *Caenorhabditis elegans*. Mutat Res 495:81–88.

140. Hoyos-Manchado R, Jimenez J, Tallada VA. 2018. Mutational analysis of N-ethyl-N-nitrosourea (ENU) in the fission yeast *Schizosaccharomyces pombe*. bioRxiv https://doi.org/10.1101/486266.

141. Peabody GLV, Li H, Kao KC. 2017. Sexual recombination and increased mutation rate expedite evolution of *Escherichia coli* in varied fitness landscapes. Nat Commun 8:2112.

142. Uphoff S. 2018. Real-time dynamics of mutagenesis reveal the chronology of DNA repair and damage tolerance responses in single cells. Proc Natl Acad Sci 115:E6516–E6525.

143. Gavande NS, Vandervere-Carozza PS, Hinshaw HD, Jalal SI, Sears CR,

Pawelczak KS, Turchi JJ. 2016. DNA repair targeted therapy: The past or future of cancer treatment? Pharmacol Ther 160:65–83.

144. Shibai A, Takahashi Y, Ishizawa Y, Motooka D, Nakamura S, Ying BW, Tsuru S. 2017. Mutation accumulation under UV radiation in Escherichia coli. Sci Rep 7:14531.

145. Gurumurthy CB, Grati M, Ohtsuka M, Schilit SLP, Quadros RM, Liu XZ. 2016. CRISPR: a versatile tool for both forward and reverse genetics research. Hum Genet 135:971–976.

146. Bermejo-Rodríguez C, Pérez-Mancera PA. 2015. Use of DNA transposons for functional genetic screens in mouse models of cancer. Curr Opin Biotechnol 35:103–110.